Pak.j.stat.oper.res. Vol.20 No. 4 2024 pp 693-718 DOI: http://dx.doi.org/10.18187/pjsor.v20i4.4302

Pakistan Journal of Statistics and Operation Research

A Novel Reciprocal-Weibull Model for Extreme Reliability Data: Statistical Properties, Reliability Applications, Reliability PORT-VaR and Mean of Order P Risk Analysis

Wahid A. M. Shehata[1], Abdussalam Aljadani[2] and Mahmoud M. Mansour[3,4], Hleil Alrweili[5,*] Mohamed S. Hamed[4,6] and Haitham M. Yousof[4]

* Corresponding Author

[1]Department of Mathematics, Statistics and Insurance, Faculty of Business, Ain Shams University, Egypt; wahid75maher@yahoo.com
[2]Department of Management, College of Business Administration in Yanbu, Taibah University, Al-Madinah, Al-Munawarah 41411, Kingdom of Saudi Arabia; ajadani@taibahu.edu.sa
[3]Department of Management Information Systems, Yanbu, Taibah University, Yanbu 46421, Saudi Arabia; mmmansour@taibahu.edu.sa
[4]Department of Statistics, Mathematics and Insurance, Faculty of Commerce, Benha University, Egypt; haitham.yousof@fcom.bu.edu.eg
[5]Department of Mathematics, College of Science, Northern Border University, Arar, Saudi Arabia; ∗Corresponding author: Hleil.Alrweili@nbu.edu.sa
[6]Department of Business Administration, Gulf Colleges, KSA; mssh@gulf.edu.sa

Abstract

Peaks over a random threshold value-at-risk (PORT-VaR) analysis is a powerful tool for evaluating extreme value reliability data, particularly for materials like carbon and glass fibers. By incorporating random thresholds into traditional value at risk (VaR) and tail value at risk (TVaR) frameworks, it provides a more nuanced understanding of how materials behave under extreme conditions, making it invaluable for applications where failure is costly or dangerous, such as aerospace, automotive, and civil engineering. The combination of Mean of Order P (MO-P), VaR and PORT-VaR analyses in medical data offers important insights into risk evaluation and patient management. By examining both average and extreme strength of glass fibers, healthcare professionals can create more effective treatment plans, enhance patient outcomes, and improve overall care quality. This comprehensive approach enables more sophisticated decision-making and targeted interventions in clinical settings. To illustrate our main objective and conduct a medical analysis, we introduced a new extreme value model called the generalized Rayleigh reciprocal-Weibull (GR-RW) and presented its key mathematical results. Additionally, we conducted a simulation study and analyzed two real datasets to compare the competing models.

Key Words: Mean of Order P; Value-at-Risk; Peaks over a random threshold value-at-risk; Reciprocal-Weibull; Reliability Applications; Risk Analysis.

1.Inroduction

The Reciprocal-Weibull (RW) distribution, as one of the three primary extreme value distributions, plays a key role in modeling rare and impactful events, and its relevance is growing in medical data analysis. Its strength lies in its capacity to model tail behavior, making it highly useful for studying infrequent but significant events, such as extreme patient outcomes, the severity of diseases, and the longevity of patients. In medical research, these extreme outcomes, such as severe reactions to treatments or critical medical events, are often rare but pose substantial risks. The RW distribution's heavy-tailed nature provides an effective tool for modeling these events, as it accurately captures their probability.

In survival analysis, for instance, the RW distribution is commonly employed to estimate extreme lifespans or survival durations of patients with chronic conditions. In cases such as cancer or cardiovascular disease, where treatment outcomes can vary dramatically, the RW distribution helps in understanding and predicting extreme strength of glass fibers, improving risk assessments and treatment plans (Kotz & Nadarajah, 2000; Harrison & Marden, 2020). This is particularly relevant in regions like the Middle East, where chronic illnesses like diabetes and heart disease are prevalent and present extreme variations in patient outcomes.

Additionally, the RW distribution is applied to model the upper tail of disease severity data, helping researchers predict worst-case scenarios. For instance, in epidemiological studies focusing on extreme complications, such as the progression of severe COVID-19 cases or rare but critical outcomes in genetic disorders, this modeling helps guide personalized treatments. In countries with high rates of non-communicable diseases, such as Saudi Arabia, modeling extreme values of disease biomarkers can help identify patients at high risk, leading to more targeted and effective treatment strategies.

The reliability of medical devices, like pacemakers or dialysis machines, is another domain where the RW distribution proves invaluable. These devices are often lifesaving, and the ability to model the time to extreme events—such as device failure—is critical. The RW distribution helps quantify the likelihood of rare but catastrophic failures, a key factor in ensuring the reliability of medical devices in healthcare systems across regions with advanced medical infrastructure, like the UAE or Kuwait (Hamedani & Maadooliat, 2021).

Furthermore, as noted by Wang and Hu (2019), the RW distribution has become widely used in survival analysis, particularly when studying extreme lifetimes, whether short or long. This is especially important in aging populations, such as in Oman, where life expectancy is rising due to advances in healthcare. The RW distribution is highly effective in capturing the tail behavior of strength of glass fibers, making it useful in studying elderly patients or those undergoing life-extending treatments. By modeling these extremes, healthcare systems can better allocate resources and optimize treatment for the most vulnerable patient groups. The probability density function (PDF) and cumulative distribution function (CDF) of the RW distribution are given by (for $\boldsymbol{y} \geq 0$)

$$g_c(y) = cy^{-(c+1)}\, exp(-y^{-c}), \tag{1}$$

and

$$G_c(y) = exp(-y^{-c}), \tag{2}$$

respectively, where $c > 0$ is a shape parameter and refers to the RW scale parameter.
The parameter governs how quickly the exponential term decays near zero. Larger values of result in a sharper decay near zero, leading to a more peaked distribution around small value of $\boldsymbol{y}$. Following Yousof et al. (2017), we defined a new flexible CDF called the generalized Rayleigh G (GR-G) family of probabilistic distribution (for $\boldsymbol{y} \in$ R) by

$$F_{a,b,\boldsymbol{\Phi}}(y) = \{1 - exp[\boldsymbol{O}_{b,\boldsymbol{\Phi}}(y)]\}^a, \tag{3}$$

where $a > 0$ is the shape parameter, $\boldsymbol{\Phi}$ is a parameters vector of base line model and

$$\boldsymbol{O}_{b,\boldsymbol{\Phi}}(y) = -b[G_{\boldsymbol{\Phi}}(y)/\bar{G}_{\boldsymbol{\Phi}}(y)]^2,$$

Where b is an additional scale parameter, the two function $\bar{G}_{\boldsymbol{\Phi}}(y)$ and $G_{\boldsymbol{\Phi}}(y)$ refers to the reliability function (RF) and the CDF of the base line model. Then, the PDF of the GR-G can be expressed as

$$f_{a,b,\boldsymbol{\Phi}}(y) = 2ab\,\frac{g_{\boldsymbol{\Phi}}(y)G_{\boldsymbol{\Phi}}(y)}{\bar{G}_{\boldsymbol{\Phi}}(y)^3}\, exp[\boldsymbol{O}_{b,\boldsymbol{\Phi}}(y)]\,\{1 - exp[\boldsymbol{O}_{b,\boldsymbol{\Phi}}(y)]\}^{a-1} \tag{4}$$

Using (2), the CDF and the PDF of the GR-RW can be derived as

$$F_{a,b,c}(y) = \{1 - exp[\boldsymbol{O}_{b,c}(y)]\}^a \tag{5}$$

and

$$f_{a,b,c}(y) = 2abc\,\frac{y^{-(c+1)}\, exp[-2y^{-c} + \boldsymbol{O}_{b,c}(y)]}{\{1 - exp[-y^{-c}]\}^3}\left[1 - exp\left(\boldsymbol{O}_{b,c}(y)\right)\right]^{a-1} \tag{6}$$

respectively, where

$$\boldsymbol{O}_{b,c}(y) = -b[exp(y^{-c}) - 1]^{-2}.$$

The parameter a mainly influences the overall shape by controlling the height and tail behavior. Larger values of a cause the distribution to have more mass in the tail. The parameter b adjusts the scaling of the distribution and can be thought of as affecting the spread. A larger b leads to a wider distribution. The distribution peaks near zero, especially for large a and c. The PDF is typically right skewed, with a heavy or light tail depending on c. The exact shape of the density function depends on the interaction of the parameters a, b, c but generally, the PDF peaks near small values and has a heavy or light tail depending on c. The term $\boldsymbol{O}_{b,c}(y)$ tends to 0 as $y \to \infty$, since $exp(y^{-c}) \to 1$.

Similarly, $\left[1 - exp\left(\boldsymbol{O}_{b,c}(y)\right)\right]^{a-1}$ will asymptotically behave as a constant since $\boldsymbol{O}_{b,c}(y)$ tends to 0. For large values of y, the leading order approximation of the PDF is

$$f_{a,\mathscr{b},c}(\mathscr{y}) \sim C\,\frac{1}{\mathscr{y}^{-3c}}\mathscr{y}^{-(c+1)},$$

where C is a constant (involving $a, \mathscr{b}, c$). Simplifying

$$f_{a,\mathscr{b},c}(\mathscr{y}) \sim C\mathscr{y}^{c-1}.$$

The tail index TI is determined by the power-law behavior of the PDF. The PDF decays as $\mathscr{y}^{\mathrm{TI}-1}$ for large $\mathscr{y}$, so from the expression $\mathscr{y}^{c-1}$, we have

$$\mathrm{TI} = 1 - c.$$

The tail index of the GR-RW distribution is $\mathrm{TI} = 1 - c$. This indicates that for $c < 1$, the distribution has a heavier tail (i.e., it decays more slowly), while for $1 < c$, the tail decays faster, leading to a lighter tail. The parameter c therefore plays a crucial role in determining the heaviness of the distribution's tail.

Over the past decade, interest in extreme value theory and its applications in areas such as medicine, engineering, insurance, and risk management has increased. Korkmaz et al. (2017) examined the odd Lindley Reciprocal Weibull distribution, while Haq et al. (2017) introduced a five-parameter model to enhance extreme value modeling. Yousof et al. (2018) created a flexible distribution incorporating regression for extreme data. Chakraborty et al. (2019) presented a new model for heavy-tailed data, particularly useful in hydrology and finance. Jahanshahi et al. (2019) developed the Burr-type X Reciprocal Weibull distribution for extreme data, and Elgohari and Yousof (2021) utilized copulas to address multivariate extremes. More recently, Almazah et al. (2023) and Yousof et al. (2023) improved models for skewed and insurance data, while Minkah et al. (2023) and Alizadeh et al. (2024) focused on extreme quantile estimation and stress analysis. For additional findings, refer to Yousof et al. (2016), Afify et al. (2016), Yousof et al. (2020, 2019, 2018a,b,c), Elsayed and Yousof (2020), Salah et al. (2020), Ibrahim et al. (2021), Ahmed and Yousof (2023), and Al-babtain et al. (2020a,b).

We provide a very useful linear representation for the GR-RW density function. If $\left|\frac{\phi_1}{\phi_2}\right| < 1$ and $\phi_3 > 0$ is a real non-integer, the power series holds

$$\left(1 - \frac{\phi_1}{\phi_2}\right)^{\phi_3 - 1} = \sum_{\ell}^{+\infty} \left(\frac{\phi_1}{\phi_2}\right)^{\ell} \frac{(-1)^{\ell}\Gamma(\phi_3)}{\ell!\,\Gamma(\phi_3 - \ell)}. \tag{7}$$

Applying (7) to last term in (6) we get

$$f_{a,\mathscr{b},c}(\mathscr{y}) = 2a\mathscr{b}c\mathscr{y}^{-(c+1)}\frac{exp(-2\mathscr{y}^{-c})}{[1 - exp(-\mathscr{y}^{-c})]^3}\sum_{\ell}^{+\infty} exp\left[(\ell+1)\boldsymbol{\mathcal{O}}_{\mathscr{b},c}(\mathscr{y})\right] \tag{8}$$

Applying the power series to the term $A_{\mathscr{b},c}(\mathscr{y};\ell)$, where

$$A_{\mathscr{b},c}(\mathscr{y};\ell) = exp\left((\ell+1)\boldsymbol{\mathcal{O}}_{\mathscr{b},c}(\mathscr{y})\right).$$

Then, equation (8) becomes

$$f_{a,\mathscr{b},c}(\mathscr{y}) = 2a\mathscr{b}c\mathscr{y}^{-(c+1)}\,exp(-2\mathscr{y}^{-c})\sum_{\ell,m}^{+\infty}\frac{(-1)^{\ell+m}[\mathscr{b}(\ell+1)]^m\Gamma(a)}{\ell!\,m!\,\Gamma(a-\ell)}\frac{exp[-(2m+1)\mathscr{y}^{-c}]}{[1 - exp(-\mathscr{y}^{-c})]^{2m+3}} \tag{9}$$

Consider the series expansion

$$\left(1 - \frac{\phi_1}{\phi_2}\right)^{-\phi_3} = \sum_{w}^{+\infty}\left(\frac{\phi_1}{\phi_2}\right)^{w}\frac{\Gamma(\phi_3 + w)}{w!\,\Gamma(\phi_3)},\ \left|\frac{\phi_1}{\phi_2}\right| < 1,\ \phi_3 > 0 \tag{10}$$

Applying the expansion in (10) to (9) for the term $B_c(\mathscr{y};m)$, where

$$B_c(\mathscr{y};m) = \{1 - exp[-\mathscr{y}^{-c}]\}^{2m+3},$$

equation (9) becomes

$$f_{a,\mathscr{b},c}(\mathscr{y}) = \sum_{m,w}^{+\infty}\boldsymbol{\Psi}_{m,w}\,h_{2m+w+2}(\mathscr{y};a,\mathscr{b},c) \tag{11}$$

where

$$\boldsymbol{\Psi}_{m,w} = 2ab\ \frac{(-1)^m \Gamma(a)\Gamma(2m+w+3)}{m!\, w!\, \Gamma(2m+3)(2m+w+2)} \sum_{\ell}^{+\infty} \frac{(-1)^{\ell}[b(\ell+1)]^m}{\ell!\, \Gamma(a-\ell)},$$

and $h_{2m+w+2}(y;a,b,c)$ is the RW density with scale parameter $(2m+w+2)^{\frac{1}{c}}$ and shape parameter c. Thus, the GR-RW density can be expressed as a double linear mixture of Fr densities. So, several of its structural properties can be obtained from Equation (11). By integrating Equation (11), the CDF of X can be given in the mixture form

$$F_{a,b,c}(y) = \sum_{m,w}^{+\infty} \boldsymbol{\Psi}_{m,w}\ \boldsymbol{\mathcal{H}}_{2m+w+2}(y;a,b,c) \qquad (12)$$

where $\boldsymbol{\mathcal{H}}_{2m+w+2}(y;a,b,c)$ is the Fr CDF with scale parameter $(2m+w+2)^{\frac{1}{c}} > 0$ and shape parameter $c > 0$.

Figure 1 (left) display some plots of the ER-Fr density for selected values of a, b, c. The density plots show that the GR-RW distribution can exhibit both symmetry and right-skewness, with a wide and narrow single peak. The hazard rate function (HRF) plots for various parameter values, as shown in Figure 1 (right), demonstrate that the GR-RW HRF can take on different shapes, including an upside-down bathtub (or upside-down-U shape), J-HRF, monotonically increasing, monotonically decreasing, and a pattern of increasing, constant, then increasing again, depending on the specific parameter values.

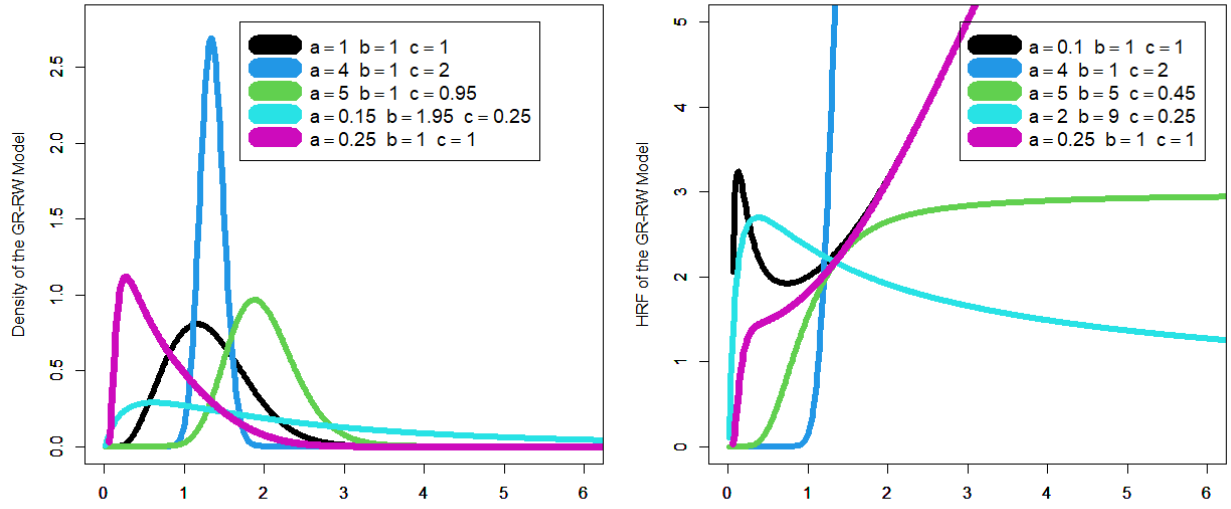

Figure 1: Density and HRF for the new model.

2. General properties

The r^{th} ordinary moment of $\boldsymbol{y}$ is given by

$$\mu'_r = E(\boldsymbol{y}^r) = \sum_{m,w}^{+\infty} \boldsymbol{\Psi}_{m,w} \int_{-\infty}^{\infty} y^r h_{2m+w+2}(y;a,b,c)dy$$

Then we obtain

$$\mu'_r = \sum_{m,w}^{+\infty} \boldsymbol{\Psi}_{m,w}\ (2m+w+2)^{\frac{r}{c}} \Gamma\left(1-\frac{r}{c}\right), \forall\, r < c, \qquad (14)$$

setting $r = 1$ in (14), we have the mean of $\boldsymbol{y}$.

The s^{th} incomplete moment, say $I_s(t)$, of $\boldsymbol{Y}$ can be expressed from (11), for $r < c$, as

$$I_s(t;\boldsymbol{Y}) = \sum_{m,w}^{+\infty} \boldsymbol{\Psi}_{m,w} \int_{-\infty}^{t} y^s h_{2m+w+2}(y;a,b,c)dy,$$

Which finally can be expressed as

$$I_s(t;\boldsymbol{Y}) = \sum_{m,w}^{+\infty} \boldsymbol{\Psi}_{m,w} (2m+w+2)^{\frac{s}{c}} \Gamma\left(1-\frac{s}{c}, (2m+w+2)\left(\frac{1}{t}\right)^c\right), \forall\, s < c, \tag{15}$$

where $\Gamma\left(1-\frac{1}{c}, (2m+w+2)\left(\frac{1}{y(\boldsymbol{U})}\right)^c\right)$ is the lower gamma function. The general formula for $I_1(t)$ (the first incomplete moment) can be obtained from $I_s(t)$ as

$$I_1(t;\boldsymbol{Y}) = \sum_{m,w}^{+\infty} \boldsymbol{\Psi}_{m,w} (2m+w+2)^{\frac{1}{c}} \Gamma\left(1-\frac{1}{c}, (2m+w+2)\left(\frac{1}{t}\right)^c\right).$$

The quantile function of the new model can be expressed as

$$y(\boldsymbol{U}) = \left\{ \ln\left[1 + \sqrt{\frac{b}{-\ln\left(1-\boldsymbol{U}^{\frac{1}{a}}\right)}}\right]\right\}^{\frac{1}{c}}. \tag{16}$$

where $\boldsymbol{U} \in (0,1)$ represents the probability level, and a, b, c are the model parameters. The quantile function $y(\boldsymbol{U})$ provides a way to map probabilities $\boldsymbol{U}$ to the corresponding quantile values y, which gives insights into the distribution's structure at different probability levels. This is crucial for applications like Value at Risk (VaR) and Tail Value at Risk (TVaR) in financial and risk analysis, as it helps identify extreme values in the tail of the distribution. This quantile function is particularly useful in extreme value modeling, where capturing the behavior of a distribution's tail is crucial. The heavy-tailed nature of the quantile function is indicative of its utility in applications involving insurance, reliability analysis, and finance, where extreme outcomes (such as rare events or failures) need to be carefully modeled and quantified.

3. Maximum likelihood estimation

In this section, we present a comprehensive procedure for maximum likelihood estimation (MLE) of the GR-RW model. This approach not only facilitates parameter estimation but also enhances our understanding of the underlying distributional properties of the GR-RW model. To rigorously evaluate the efficacy of the MLEs, we conduct a simulation study, varying the sample sizes to observe how these estimators perform under different conditions. This analysis is crucial, as it allows us to assess the robustness and reliability of the MLEs, ultimately informing their application in real-world scenarios. We utilize the MLEs derived from our analysis to model two real datasets, applying the GR-RW distribution alongside other comparative distributions. This comparative approach helps to elucidate the advantages and potential limitations of the GR-RW model in capturing the essential characteristics of the data. Our focus on estimating the unknown parameters of the GR-RW model is exclusively based on complete samples, ensuring that our methodology adheres to the principles of maximum likelihood. The MLEs for the parameters of the GR-RW model will be examined in detail. Consider a random sample represented by $y_1, \ldots, y_n$, which follows the GR-RW distribution characterized by the parameter vector $\boldsymbol{\psi} = (a, b, c)^T$. The log-likelihood function for this parameter vector, denoted as $\ell = \ell(\boldsymbol{\psi})$, is formulated as follows

$$\begin{aligned}\ell = {} & n\,log(2) + n\,log(a) + n\,log(b) + n\,log(c) - (c-1)\sum_{\ell=1}^{n} log(y_\ell) \\ & + \sum_{\ell=1}^{n}\left[-2\left(\frac{1}{y_\ell}\right)^c - b\left(\frac{V_\ell}{1-V_\ell}\right)^2\right] - 3\sum_{\ell=1}^{n} log(1-z_\ell) \\ & + (a-1)\sum_{\ell=1}^{n} log\left\{1 - exp\left[-b\left(\frac{V_\ell}{1-V_\ell}\right)^2\right]\right\},\end{aligned}$$

where $V_\ell = exp[-y_\ell{}^c]$. This log-likelihood function encompasses various components, each contributing to the overall estimation of the parameters a, b, and c.

The maximization of this log-likelihood function can be achieved through several computational programs. For instance, in R, the optimization can be efficiently performed using the optim function, while SAS offers the PROC NLMIXED procedure for similar purposes. Alternatively, one can derive and solve the nonlinear likelihood equations obtained by differentiating $\ell(\boldsymbol{\psi})$ to find the optimal parameter estimates. The overall objective of this section is to establish a reliable estimation framework for the GR-RW model, ensuring that practitioners can accurately infer model parameters from empirical data. By thoroughly discussing the MLEs and their computational aspects, we aim to provide a solid foundation for future applications of the GR-RW model in various fields, especially where extreme value analysis is pivotal. This procedure not only enhances the theoretical understanding of the model but also bridges the gap between statistical theory and practical application, ensuring that the GR-RW model can be effectively utilized in real-world scenarios.

4. Performance of MLEs

In this subsection, we undertake a comprehensive simulation study using R to assess the performance of the maximum likelihood estimators (MLEs) for the Generalized Rayleigh reciprocal-Weibull (GR-RW) model. The focus of our investigation is to analyze how varying sample sizes impact the efficiency and accuracy of the MLEs. To ensure a robust evaluation, we present simulations across multiple sample sizes, specifically $n = 50, 100, \ldots, 1000$. The process of simulating random variables from well-defined probability distributions has been extensively documented in the computational statistics literature. Among the various techniques available, methods such as the inverse transformation method and rejection sampling are commonly employed. In the context of the GR-RW distribution, the inverse transformation method proves to be particularly effective due to its straightforward implementation and computational efficiency. To simulate random variables $\boldsymbol{y}$ from the GR-RW distribution, we follow these systematic steps:

I. Set the sample size n and the parameter vector $\boldsymbol{\psi}$=(a, b, c).
II. Simulate $\boldsymbol{u} \sim U(0,1)$, which represents uniformly distributed random variables.
III. Generate the variable yy using the inverse cumulative distribution function (CDF) method, as defined by Equation (16).
IV. Repeat the above steps nn times to obtain a complete dataset $y_1, y_2, \ldots, y_n$ from the GR-RW distribution characterized by parameters a, b, c).

For the simulation study, we utilize specific parameter values $a = 10.5$, $b = 1.25$ and $c = 0.05$. These values were chosen to represent a realistic scenario within the context of our modeling objectives. The Monte Carlo simulations are executed 2000 times, enabling us to gather sufficient data for a comprehensive analysis of the MLEs. After generating the samples, we assess the performance of the MLEs based on two key metrics: bias and mean squared errors (MSEs). These metrics provide valuable insight into the accuracy and precision of our parameter estimates. The calculations of bias and MSE are performed using R, which offers robust statistical capabilities for handling such analyses. The empirical results of our simulations are graphically illustrated in Figures 2, allowing for a visual representation of the relationships between sample size, bias, and MSE. Notably, our findings reveal a clear trend: as the sample size increases, both the biases and MSEs demonstrate a marked decrease. This pattern indicates that the maximum likelihood estimation method is not only effective but also becomes increasingly reliable with larger sample sizes when applied to the GR-RW distribution.

For the first bias plot, this plot shows how the bias of the estimated parameter a changes as the sample size n increases. The bias appears to decrease as n grows, indicating that the estimator for θ becomes more accurate with larger sample sizes. For the first MSE plot, this plot shows the MSE for the estimator of θ as a function of n. A downward trend in MSE is visible, which indicates that the estimator becomes more reliable and consistent as the sample size increases. For the second bias plot, the bias for the parameter b (scale parameter of the new family) is plotted here. Similar to the bias of a, the bias decreases as the sample size increases. For small sample sizes, the bias fluctuates, but as n grows, the bias tends to stabilize near zero, indicating improved estimation accuracy. For the second MSE plot), this plot depicts the MSE for the b parameter estimator. A noticeable decline in MSE occurs as the sample size n grows, reflecting that larger samples lead to more precise estimates of b. For the third bias plot, this plot shows the bias in estimating c (the shape parameter). Similar to the other parameters, the bias decreases as the sample size increases,

indicating that the estimator becomes more accurate for larger n. The bias fluctuates for small n, but stabilizes around zero with larger sample sizes. The red horizontal line at zero represents no bias. The plot suggests that, for small n, the bias is higher, but the estimator stabilizes as n increases. The last plot shows the MSE for the estimator of c as a function of n. Like the MSE for the other parameters, it decreases as the sample size grows, indicating greater precision of the estimator as n increases.

For all parameters $(a, \mathscr{b}, c)$, the bias decreases as the sample size increases. This suggests that the estimators for these parameters become unbiased for larger samples, a desirable property in statistical estimation. The MSE values for all three parameters also show a decreasing trend as n increases. This indicates that, as more data is available, the variance and overall error of the parameter estimates reduce, leading to more reliable and accurate models.

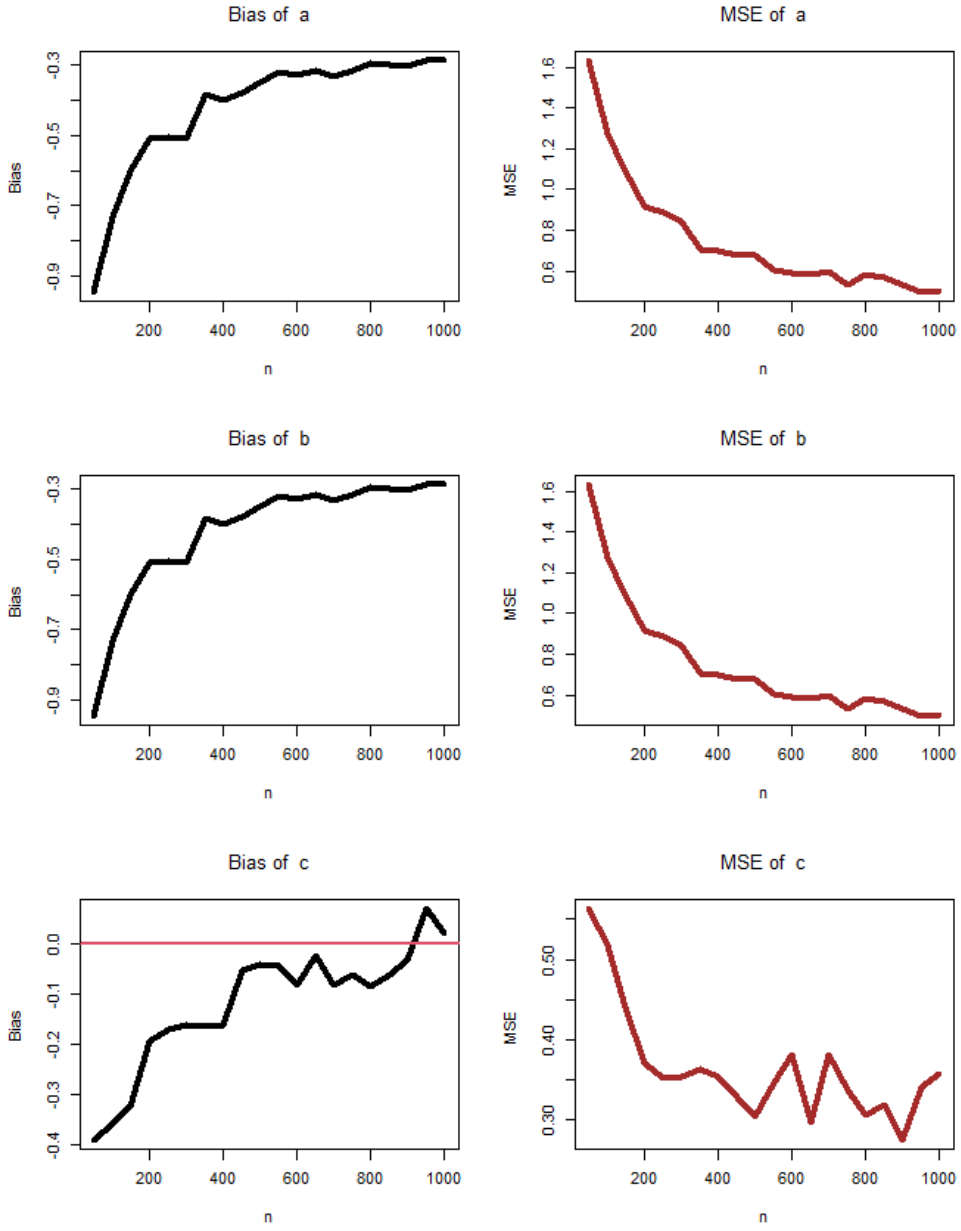

Figure 2: The simulation results.

5.Real data modelling

To demonstrate the broad applicability of the new GR-RW model, we consider several goodness-of-fit statistics: the Cramér–von Mises (C1) statistic, the Anderson–Darling (C2) statistic, the Kolmogorov–Smirnov (K-S) statistic, along with its corresponding p-value ("P-V"). Table 6 presents a comparison with competing models. The models included in the comparison are: the transmuted reciprocal-Weibull (T-RW), exponentiated reciprocal-Weibull (E-RW), beta reciprocal-Weibull (B-RW), Marshal–Olkin reciprocal-Weibull (MO-RW), McDonald reciprocal-Weibull (Mc-RW), odd log-logistic reciprocal-Rayleigh (OLL-IR), the standard reciprocal-Weibull (SRW), odd log-logistic exponentiated reciprocal-Weibull (OLL-E RW), Odd Log-Logistic exponentiated reciprocal-Rayleigh (OLL-EIR), and generalized odd log-logistic reciprocal-Rayleigh (GOLL-IR).

5.1. Stress Data

The first dataset under consideration consists of 100 uncensored observations measuring the breaking stress of carbon fibers, expressed in gigapascals (GPa). These data were originally reported by Nichols and Padgett (2006) and serve as a valuable resource for studying the mechanical properties of carbon fibers under stress. Understanding the breaking stress of materials like carbon fibers is critical for industries such as aerospace and automotive, where these fibers are widely used for their strength and lightweight properties. To explore the behavior of the empirical hazard rate function (HRF) of the dataset, a total time on test (TTT) plot is presented in Figure 3(I). The TTT plot is a commonly used tool in reliability analysis to assess the failure rate pattern of a dataset. From this plot, it is evident that the empirical HRF follows a "monotonically increasing" trend. This indicates that as time progresses, or as stress increases, the likelihood of failure (i.e., the hazard rate) rises. In practical terms, this suggests that the carbon fibers become more prone to failure under higher levels of stress, an expected behavior for many materials subjected to mechanical loads.

In addition to the HRF, further analysis is performed to understand the underlying distribution of the data. A non-parametric Kernel Density Estimation (KDE) is provided in Figure 3(II), which offers insights into the shape of the data distribution without assuming any specific parametric form. The KDE reveals that the data distribution is "asymmetrically right skewed with a heavy tail." This right-skewness suggests that most carbon fibers have relatively low breaking stress values, but a smaller portion of fibers can withstand significantly higher stress levels. The heavy tail further indicates the presence of extreme values or outliers on the higher end of the distribution, which may correspond to exceptionally strong fibers. To examine these extreme values more closely, a box plot is displayed in Figure 3(III). The box plot is a useful tool for detecting outliers and understanding the spread of the data. The plot highlights the existence of several extreme values that deviate from the central mass of the data. These extreme values likely represent carbon fibers that can endure much greater stress than the average fiber. The presence of such outliers can be important for material selection in applications that require high durability under stress. Finally, the Quantile-Quantile (Q–Q) plot in Figure 3(IV) is used to confirm the presence of outliers and to assess how well the data conforms to a theoretical distribution, such as the normal distribution. The Q–Q plot compares the quantiles of the observed data with those of a reference distribution, and deviations from the line suggest departures from the expected distribution. In this case, the Q–Q plot reinforces the finding from the box plot, showing that the dataset contains significant extreme values, further affirming the heavy-tailed nature of the distribution. Together, these visualizations offer a comprehensive view of the dataset, highlighting its key features such as the increasing hazard rate, right-skewed distribution, and the presence of extreme values, all of which are important for understanding the reliability and failure behavior of carbon fibers under stress.

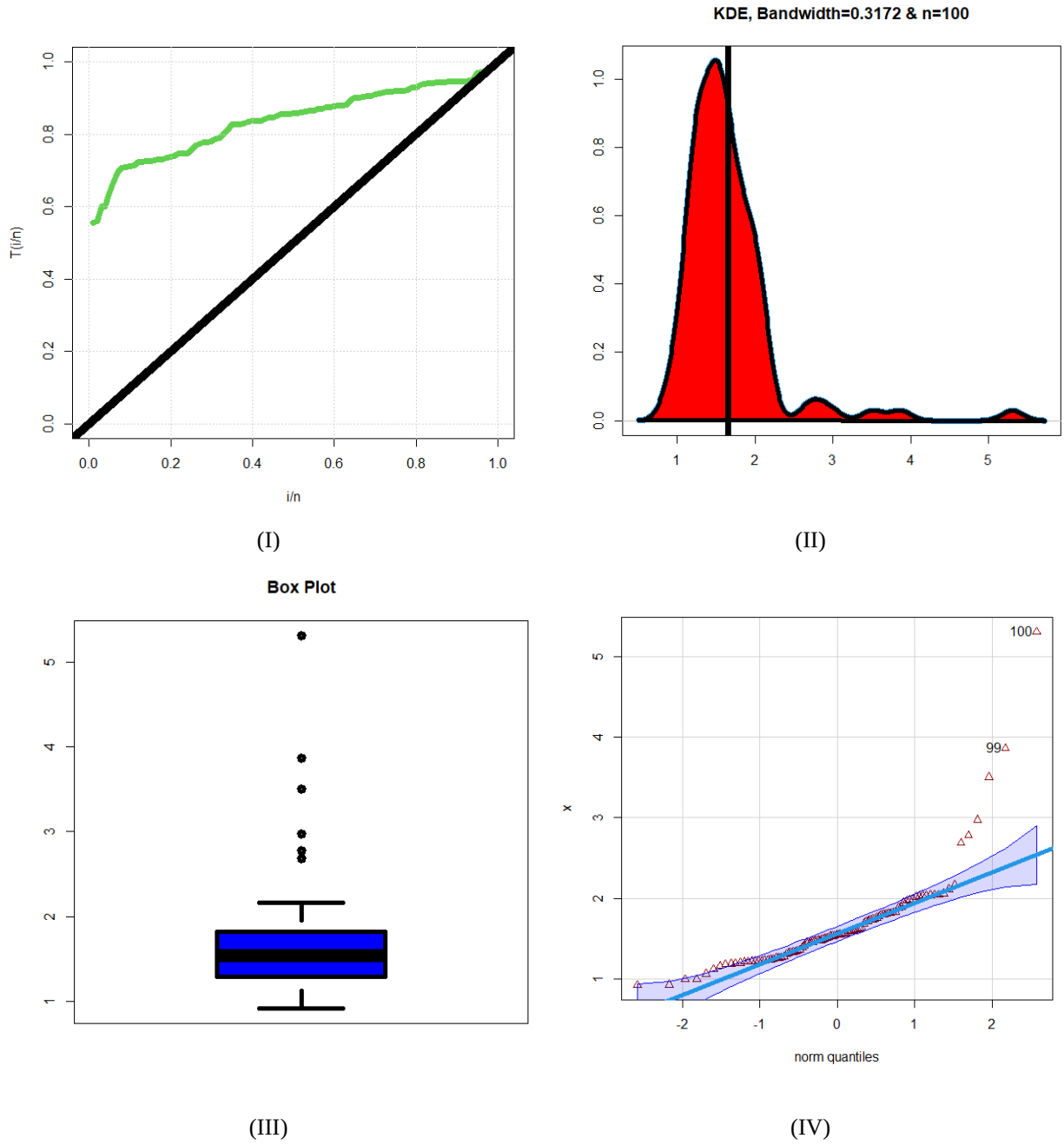

(I) (II)

(III) (IV)

Figure 3: (I) TTT plot; (III) KDE plot; (III) box plot; (IV) Q–Q plot for breaking stress of carbon fibers.

Table 1 presents the goodness-of-fit criteria, including the C1, C2, K-S, and p-value (P-V) statistics for various models applied to breaking stress of carbon fibers. The GR-RW model has the lowest C1 value (0.08606), indicating a better overall fit compared to the other models. Lower C1 values suggest that the empirical distribution of the data is closer to the theoretical distribution proposed by the GR-RW model. The GR-RW model also exhibits a competitive C2 value (0.68667), which is lower than most other models. A smaller C2 statistic indicates a better fit, especially in the tails of the distribution, which is important when modeling tail-heavy data like this. With a K-S value of 0.08139, the GR-RW model shows the smallest deviation between the empirical and theoretical cumulative distribution functions (CDF). A lower K-S statistic suggests a stronger

goodness of fit. The GR-RW model also has the highest p-value (0.52162), well above the commonly used significance threshold of 0.05. This high p-value indicates that there is no significant difference between the observed and expected distributions under the GR-RW model, affirming its suitability for this data set. In contrast, the other models, particularly the OLL-ERW, OLL-ERR, and OLL-RR, perform much worse, with much larger C1, C2, and K-S values. Moreover, these models yield extremely small p-values (2×10^{-16}), implying a significant discrepancy between the observed data and the expected distribution, which makes them unsuitable for modeling this dataset. The RW and MO-RW models also provide relatively good fits, as indicated by their moderate C1, C2, K-S values, and reasonably high p-values. However, they are still outperformed by the GR-RW model in every goodness-of-fit criterion.

Table 2 presents the maximum likelihood estimates (MLEs) along with their standard errors (in parentheses) for various models applied to breaking stress of carbon fibers. The parameters of each model differ, but they collectively aim to describe the underlying distribution of the data, particularly in terms of fitting the breaking stress of carbon fibers. Overall, the GR-RW model consistently demonstrates high precision with smaller standard errors across its parameters, reinforcing its position as the best-fitting model for this dataset. The low standard errors reflect a high level of confidence in the estimates, suggesting that the model is well-calibrated to capture the distribution of the breaking stress of carbon fibers. In contrast, models such as OLL-EIR and OLL-IR show higher uncertainty in their estimates, making them less reliable for this data. Other models like RW and MO-RW offer moderately good fits but are still outperformed by the GR-RW model in terms of precision and overall fit. Figure 4 presents the estimated density(I); (II) estimated cumulative distribution function (CDF) for breaking stress of carbon fibers.

Table 1: C1, C2, K-S and P-V for breaking stress of carbon fibers.

Model	**Goodness of Fit Criteria**			
	C1	C2	K-S	P-V
GR-RW	**0.08606**	**0.68667**	**0.08139**	**0.52162**
OLL-ERW	0.12034	0.96399	0.55615	2×10^{-16}
OLL-ERR	0.15535	1.21196	0.65496	2×10^{-16}
OLL-RR	0.15533	1.21201	0.65503	2×10^{-16}
SRW	0.10906	0.76577	0.08746	0.42818
E-RW	0.10917	0.76577	0.08749	0.42867
MO-RW	0.08868	0.61424	0.07639	0.51684

Table 2: MLEs and their standard errors (in parentheses) for breaking stress of carbon fibers.

Model	**Estimates**				
	$\hat{a}$	$\hat{b}$	$\hat{c}$	$\hat{\beta}$	$\hat{\theta}$
GR- RW	1410.2818	17.439189	0.188858		
	(1.351944)	(2.798037)	(2.803×10^{-2})		
OLL-E RW	0.135143		3.721643	0.92964	21.3197
	(0.01154)		(0.00345)	(0.00333)	(0.00346)
OLL-EIR	0.494665		0.06764	1.742625	
	(0.041353)		(0.719534)	(9.30074)	
OLL-IR	0.494595			0.452425	
	0.041356			0.038688	
SRW				1.396844	4.37245
				(0.03367)	(0.32784)
E-RW		0.939545		1.416886	0.93956
		(3.54377)		(2.5687)	(0.32786)
MO-RW		0.00336		6.22967	1.24199
		(0.00098)		(1.01344)	(0.11819)

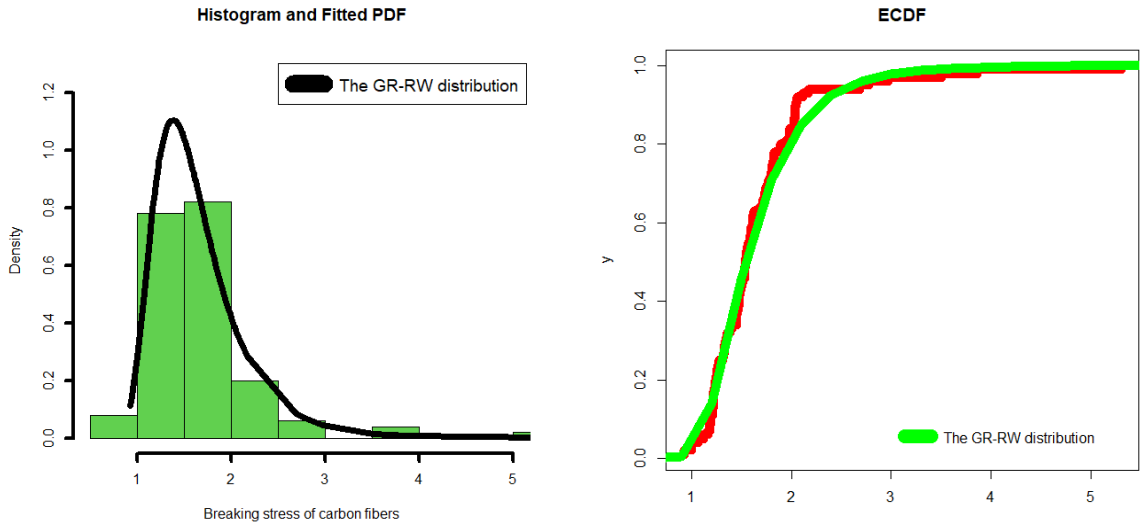

(I) (II)

Figure 4: (I) Estimated density; (II) estimated CDF for breaking stress of carbon fibers.

5.2. Glass Fibers Data

The second dataset consists of generated data designed to simulate the strength of glass fibers, as presented by Smith and Naylor (1987). This simulated dataset is intended to mimic real-world measurements of how glass fibers perform under stress, providing insights into their durability and potential failure points. Glass fibers, commonly used in applications ranging from telecommunications to construction materials, require detailed analysis of their strength characteristics to ensure reliability in practical use.

To analyze the empirical HRF of this dataset, a TTT plot is displayed in Figure 5(I). The TTT plot is a powerful tool in reliability analysis, used to visualize failure rates over time or under increasing stress conditions. From Figure 5(I), it is evident that the empirical HRF for this dataset follows a "monotonically increasing" pattern. This suggests that as stress on the glass fibers increases, so does the likelihood of failure, aligning with typical behavior seen in materials where the risk of breakage rises with greater load or use over time. Further investigation into the shape and distribution of the data is done using non-parametric methods. The KDE is provided in Figure 5(II) to explore the initial shape of the dataset without assuming any specific parametric form. The KDE reveals that the distribution of glass fiber strengths is "asymmetrically right skewed with a heavy tail." This means that while most glass fibers exhibit lower strength values, there is a noticeable spread towards higher strength values, with a small number of fibers able to withstand significantly greater stress. The presence of a heavy tail indicates that extreme values, or outliers, are present in the dataset, which could represent fibers that are unusually strong compared to the rest. To further examine these potential extreme values, a box plot is provided in Figure 5(III). The box plot is an effective way to visualize the spread of the data and identify outliers. In this case, the box plot confirms the existence of extreme values in the glass fiber strength data. These outliers represent fibers that deviate significantly from the average, highlighting the variability in the material's strength and suggesting that a few fibers can endure much more stress than most others. This kind of variability is important in materials engineering, as understanding the range of strengths helps in designing products that account for both average and extreme performance levels.

Finally, a Q–Q plot is presented in Figure 5(IV) to validate the presence of these extreme values. The Q–Q plot compares the quantiles of the observed data with those of a theoretical reference distribution, such as the normal distribution. Deviations from the straight line in the Q–Q plot indicate that the data do not perfectly align with the assumed theoretical distribution, particularly in the tails. In this case, the Q–Q plot clearly demonstrates the presence of significant outliers, consistent with the findings from the box plot and KDE. These outliers reinforce the observation that some glass fibers exhibit strength well beyond the typical range. Together, these graphical analyses provide a thorough understanding of the second dataset, highlighting its key characteristics: the increasing hazard rate, the right-skewed distribution with a heavy tail, and the presence of extreme values. This information is essential for assessing

the reliability of glass fibers under stress and understanding the full spectrum of their performance capabilities, particularly in applications that demand high durability and strength.

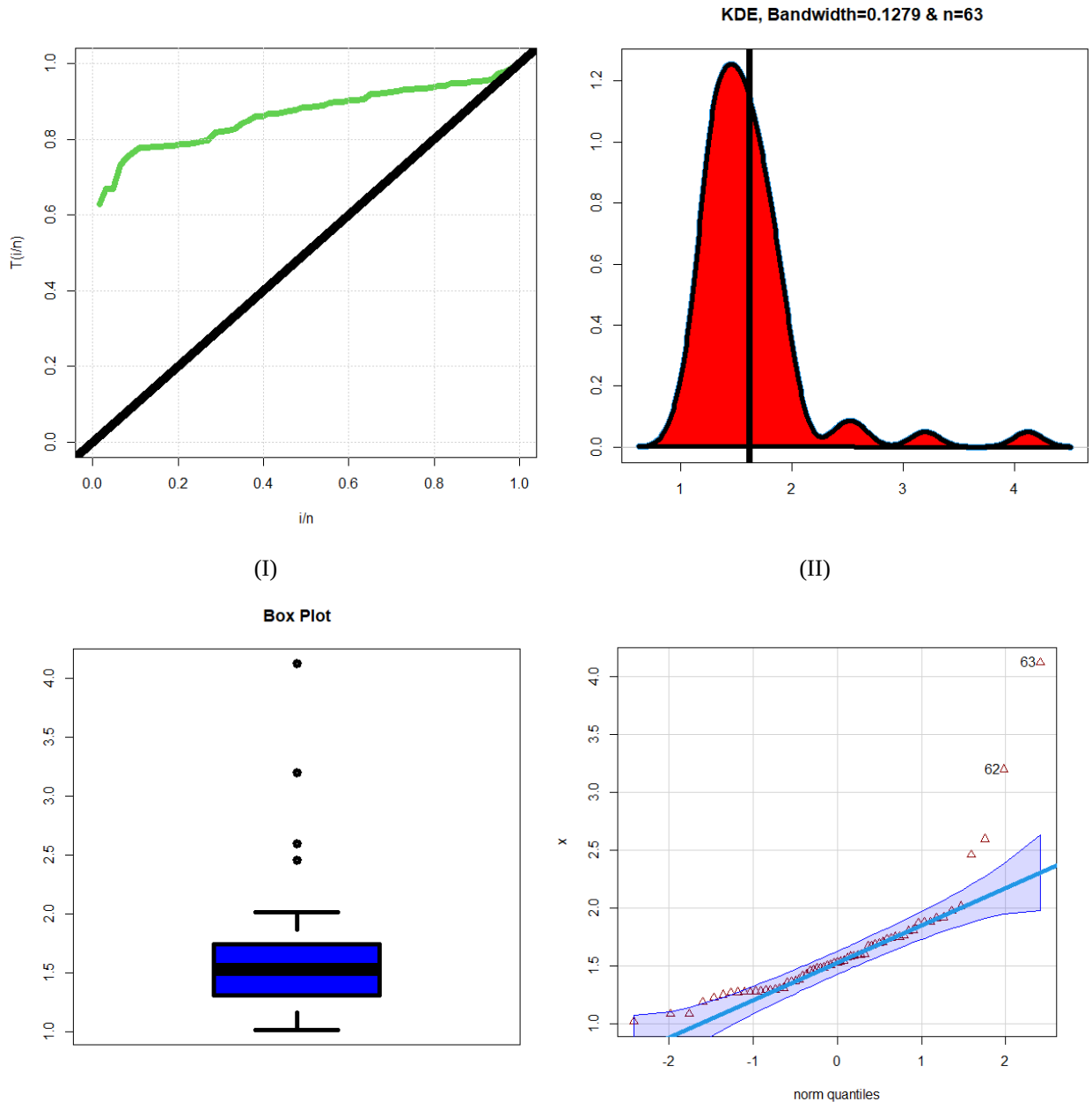

(I) (II)

(III) (IV)

Figure 5: (I) TTT plot; (III) KDE plot; (III) box plot; (IV) Q–Q plot for strength of glass fibers data.

Table 3 presents the results of various goodness-of-fit statistics (C1, C2, K-S, and P-V) for different models applied to strength of glass fibers data. These metrics are used to assess the fit of the models, with lower values of C1, C2, and K-S and higher P-V (p-values) indicating a better fit. OLL-E RW, OLL-EIR, and OLL-IR models perform significantly worse than the GR-RW model. The C1 and C2 values for these models are much higher (C1 ranging from 0.10489 to 0.15029, and C2 ranging from 0.83255 to 1.14696). Additionally, their K-S values are substantially larger, indicating a poor fit, and the extremely low p-values (on the order of 4×10^{-16}) suggest that these models do not adequately represent the data. The GR-RW model

shows the most favorable goodness-of-fit criteria across the board: C1=0.07171, C2=0.58963, K−S=0.072904, and P−V=0.8669. These values suggest that the GR-RW model closely fits the empirical distribution of the data, especially with its high p-value (0.8669), indicating a strong agreement with the data. Both the C1 and K-S values are low, and C2 is reasonable compared to the other models, making the GR-RW model the best overall fit for strength of glass fibers data. The GR-RW model is clearly the best fit for Strength of glass fibers data, as it consistently produces the lowest C1, C2, and K-S values among the competing models, alongside the highest p-value, which indicates that the model provides a highly accurate representation of the data. Other models, particularly RW, E-RW, and T-RW, offer relatively close fits but fall short when compared to the superior performance of the GR-RW model. Models like OLL-E RW, OLL-EIR, and OLL-IR perform poorly, with high C1, C2, and K-S values, and extremely low p-values, indicating that they are not suitable for this dataset.

Table 4 presents the Maximum Likelihood Estimates (MLEs) and their associated standard errors for various models applied to the strength of glass fibers data. These estimates represent the parameters of each model, with standard errors indicating the precision of these estimates. The GR-RW model once again proves to be the best-fitting model based on both the quality of its estimates and the low associated standard errors. The small standard errors suggest the stability of the GR-RW model in fitting the data, and the values of its parameters show that it can adequately capture the behavior of the glass fiber strength distribution. Figure 6 presents the estimated density (I); (II) estimated CDF for breaking stress of carbon fibersI.

Table 3: C1, C1, K-S, and P-V for strength of glass fibers data.

Model	**Goodness of Fit Criteria**			
	C1	C2	K-S	P-V
GR-RW	0.07171	0.58963	0.072904	0.8669
OLL-E RW	0.10489	0.83255	0.55194	4×10^{-16}
OLL-EIR	0.15029	1.14696	0.67943	4×10^{-16}
OLL-IR	0.15028	1.14695	0.67952	4×10^{-16}
SRW	0.07069	0.53326	0.07725	0.81846
E- RW	0.07066	0.53327	0.07727	0.81869
T- RW	0.06557	0.49399	0.07358	0.84705
MO- RW	0.06295	0.49024	0.08139	0.76849
Mc- RW	0.11614	0.91936	0.08309	0.74555

Table 4: MLEs and their standard errors (in parentheses) for strength of glass fibers data.

Model	**Estimates**				
	$\hat{a}$	$\hat{b}$	$\hat{c}$	$\hat{\beta}$	$\hat{\theta}$
GR- RW	1569.5889	16.826924	0.2316918		
	(1.759755)	(3.248488)	(4.08×10^{-2})		
OLL-E RW	0.144965		0.00886	1.29977	24.8767
	(0.01364)		(0.00002)	(0.0001)	(0.0002)
OLL-EIR	0.502563		0.07166	1.70486	
	(0.05390)		(1.13068)	(13.47)	
OLL-IR	0.502518			0.455919	
	0.052957			0.048657	
SRW				1.41087	5.43778
				(0.03449)	(0.51929)
E- RW		0.90579		1.43676	5.43794
		(2.7694)		(4.3294)	(0.51934)
B- RW		1.29969	1.26488	1.39455	4.79277
		(4.43787)	(0.66407)	(0.93048)	(1.46416)
T- RW	0.77785			1.54917	4.31379
	(0.24779)			(0.06559)	(0.58499)
MO- RW		0.00230		5.23837	1.45378
		(0.00049)		(0.82094)	(0.16504)
Mc- RW		56.2275	14.9534	0.00735	29.1049

(30.5393)	(4.7338)	(0.00138)	(11.3046)

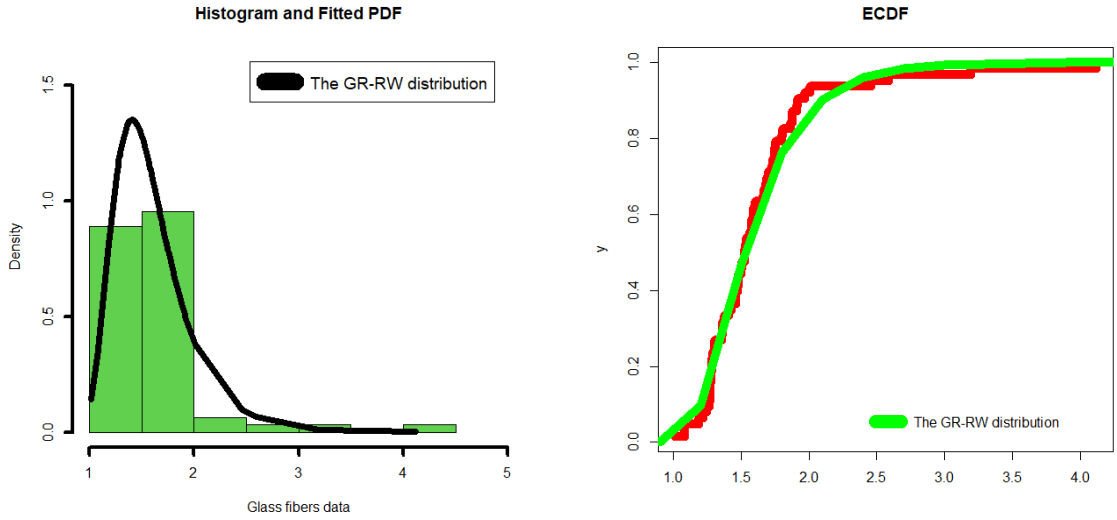

(I) (II)

Figure 5: (I) Estimated density;(II) estimated CDF for strength of glass fibers data.

5. Risk analysis and extreme reliability data

5.1 The VaR

Value at Risk (VaR) at a given confidence level $\boldsymbol{q}$ is defined as the quantile of the distribution corresponding to the probability level $\boldsymbol{q}$. Since the quantile function is denoted as $y(\boldsymbol{U})$, the VaR at level $\boldsymbol{q}$ is simply the quantile at that specific probability. To calculate VaR, we substitute $\boldsymbol{U} = \boldsymbol{q}$ into the quantile function, resulting in the following equation

$$\mathrm{VAR}|\boldsymbol{q} = y(\boldsymbol{U}) = \{\ln[1 + S(\boldsymbol{b}, a|\boldsymbol{q})]\}^{\frac{1}{c}} \tag{17}$$

Here, $S(\boldsymbol{b}, a|\boldsymbol{q})$ is given by

$$S(\boldsymbol{b}|\boldsymbol{q}) = \sqrt{\boldsymbol{b}/\left[-\ln\left(1 - \boldsymbol{q}^{\frac{1}{a}}\right)\right]}$$

This formula provides the VaR at the confidence level $\boldsymbol{q}$, where $S(\boldsymbol{b}, a|\boldsymbol{q})$ is a scaling function based on the parameter $\boldsymbol{b}$, and incorporates the logarithmic term $\ln\left(1 - \boldsymbol{q}^{\frac{1}{a}}\right)$, reflecting the tail behavior of the distribution.

5.2 The TVaR

The TVaR, also known as conditional Value at Risk (CVaR), is the expected value of the losses exceeding the VaR at the given confidence level $\boldsymbol{q}$. It is computed as the conditional expectation of the model beyond the VaR threshold. The TVaR of $\boldsymbol{Y}$ at the $100\boldsymbol{q}\%$ confidence level is the expected loss given that the loss exceeds the $100\boldsymbol{q}\%$ of the distribution of $\boldsymbol{Y}$, then the $\mathrm{TVAR}(\boldsymbol{Y}; \boldsymbol{\psi})$ of $\boldsymbol{Y}$ can be expressed as

$$\mathrm{TVaR}(\boldsymbol{Y}; \boldsymbol{\psi}) = \mathbf{E}(\boldsymbol{Y}|\boldsymbol{Y} > y(\boldsymbol{U})),$$

which can be derived form

$$\mathrm{TVaR}(\boldsymbol{Y}; \boldsymbol{\psi}) = \frac{1}{1 - F_{\boldsymbol{\psi}}(y(\boldsymbol{U}))} \int_{\pi(\boldsymbol{q})}^{\infty} y \; f_{\boldsymbol{\psi}}(y)\, dy.$$

Then,

$$\mathrm{TVaR}(\boldsymbol{y};\boldsymbol{\psi}) = \frac{1}{1-\boldsymbol{q}} \int_{y(\boldsymbol{u})}^{\infty} y\, f_{\boldsymbol{\psi}}(y)dy.$$

Then,

$$\mathrm{TVaR}(\boldsymbol{y};\boldsymbol{\psi}) = \frac{1}{1-\boldsymbol{q}} \sum_{m,w}^{+\infty} \boldsymbol{\Psi}_{m,w}\,(2m+w+2)^{\frac{1}{c}} \gamma\left(1-\frac{1}{c}, (2m+w+2)\left(\frac{1}{y(\boldsymbol{u})}\right)^{c}\right), \tag{18}$$

where

$$\gamma\left(1-\frac{1}{c}, (2m+w+2)\left(\frac{1}{y(\boldsymbol{u})}\right)^{c}\right) = \Gamma\left(1-\frac{1}{c}\right) - \Gamma\left(1-\frac{1}{c}, (2m+w+2)\left(\frac{1}{y(\boldsymbol{u})}\right)^{c}\right),$$

and the function $\gamma\left(1-\frac{1}{c}, (2m+w+2)\left(\frac{1}{y(\boldsymbol{u})}\right)^{c}\right)$ refers to the upper gamma function. Thus, the quantity $\mathrm{TVaR}(\boldsymbol{y};\boldsymbol{\psi})$ represents the average of all $\mathrm{VAR}|\boldsymbol{q}$ values beyond the specified confidence level q, capturing more comprehensive information about the behavior of the tail of the distribution. Unlike VaR, which only gives the threshold for potential losses at a given percentile, $\mathrm{TVaR}(\boldsymbol{y};\boldsymbol{\psi})$ provides insight into the magnitude of losses that can occur in the extreme tail beyond this threshold. This makes $\mathrm{TVaR}(\boldsymbol{y};\boldsymbol{\psi})$ a more informative and robust risk measure for assessing extreme events, particularly in distributions with heavy tails, such as the GR-RW distribution.

5.3 The mean excess loss function

In mathematical terms, $\mathrm{TVaR}(\boldsymbol{y};\boldsymbol{\psi})$ can be expressed as

$$\mathrm{TVaR}(\boldsymbol{y};\boldsymbol{\psi}) = \mathrm{VaR}|\boldsymbol{q} + T(\boldsymbol{y};\boldsymbol{\psi})|\boldsymbol{q} \tag{19}$$

where $T(\boldsymbol{y};\boldsymbol{\psi})|\boldsymbol{q}$ represents the mean excess loss (MEL) function evaluated at the 100q% quantile, which corresponds to $\mathrm{VaR}|\boldsymbol{q}$ at the confidence level $\boldsymbol{q}$. The MEL function reflects the expected value of losses that exceed the $\mathrm{VaR}|\boldsymbol{q}$ threshold, thereby capturing the severity of extreme losses. This decomposition highlights that $\mathrm{TVaR}(\boldsymbol{y};\boldsymbol{\psi})$ extends beyond $\mathrm{VaR}|\boldsymbol{q}$ by including the expected shortfall for losses beyond the $\mathrm{VaR}|\boldsymbol{q}$ limit.

This relationship between $\mathrm{TVaR}(\boldsymbol{y};\boldsymbol{\psi})$ and the MEL function has been extensively examined in the literature. For example, Wirch (1990) introduced early discussions on risk measures that go beyond traditional VaR, while Tasche (2002) and Acerbi and Tasche (2002) further formalized $\mathrm{TVaR}(\boldsymbol{y};\boldsymbol{\psi})$ as a coherent risk measure. Their work demonstrated that $\mathrm{TVaR}(\boldsymbol{y};\boldsymbol{\psi})$ addresses the limitations of $\mathrm{VaR}|\boldsymbol{q}$, particularly its inability to fully capture tail risks, making $\mathrm{TVaR}(\boldsymbol{y};\boldsymbol{\psi})$ a more effective tool in risk management, especially when understanding the magnitude of extreme losses is critical.

By incorporating the MEL function, $\mathrm{TVaR}(\boldsymbol{y};\boldsymbol{\psi})$ offers a more comprehensive view of risk exposure. It not only considers the probability of extreme losses but also their potential severity, which is crucial for industries such as insurance, finance, and healthcare that must effectively manage tail risks. For more details, see Tasche (2002), Acerbi and Tasche (2002), Wirch (1990), and Shrahili et al. (2021).

5.3 MO-P analysis

Due to Alizadeh et al. (2024) and Elbatal et al. (2024), The Mean of Order-P (MO-P) analysis is an important statistical tool used to assess the reliability of materials under extreme conditions, such as the breaking stress of carbon fibers and the strength of glass fibers. The MO-P measure is a generalized mean that places more emphasis on either the lower or higher values in a dataset, depending on the value of the parameter P. This flexibility makes it particularly useful for analyzing extreme value data in reliability contexts, where tail behavior is critical. In the context of extreme value reliability data, such as breaking stress or fiber strength, the MO-P helps provide insight into the behavior of materials under high-stress conditions. By adjusting the parameter P, one can focus the analysis either on the weakest fibers (if $P < 1$) or on the strongest ones (if $P > 1$), giving a nuanced view of material performance.

Carbon fibers are known for their high strength and stiffness, making them crucial in applications like aerospace and high-performance sports equipment. However, their performance can vary under extreme stress. MO-P analysis allows researchers to focus on the behavior of fibers at the extreme ends of their stress distribution.

Glass fibers are commonly used in composites due to their lightweight and high strength. Their performance in extreme conditions, such as under tension or compression, is crucial for their application in structural engineering. By applying MO-P analysis, engineers can evaluate the extreme strength distribution, focusing on different sections of the data to predict failure probabilities at the lower end of the distribution when P is less than 1, which is critical for safety standards. Also to assess maximum performance metrics at the higher end when P is greater than 1, useful for optimizing material design and ensuring high-strength applications. The MOOP is computed as

$$\mathrm{MOOP}(\boldsymbol{y};\boldsymbol{\psi}) = \left(\frac{1}{n}\sum_{i=1}^{n}\boldsymbol{y}_i^P\right)^{\frac{1}{P}}, \tag{20}$$

where $\boldsymbol{y}_i$ are the data points (such as breaking stress or fiber strength) and P is the order of the mean. As P changes, the focus shifts between different parts of the distribution.

5.5 The PORT-VaR method

The PORT-VaR analysis is a sophisticated statistical approach used to model extreme events in reliability data, especially for materials like carbon fibers and glass fibers. It is a variation of the Peaks Over Threshold (POT) method, commonly used in extreme value theory (EVT), but with an added layer of complexity by introducing randomness into the threshold selection. This allows for more flexible and accurate modeling of the tail behavior of data, which is critical in assessing the reliability of materials under extreme stress conditions. In the context of extreme value reliability data, such as the breaking stress of carbon fibers and the strength of glass fibers, PORT-VaR helps quantify the risk of extreme failures or breakdowns beyond a certain randomly defined threshold. This is particularly important in industries like aerospace, civil engineering, and manufacturing, where understanding and mitigating the risks of material failure are crucial for safety and performance. Unlike POT, where the threshold is fixed, PORT-VaR introduces a random threshold. This randomization allows the model to account for uncertainty or variability in what might be considered an extreme event. For instance, in fiber testing, environmental factors, manufacturing inconsistencies, or measurement errors may cause variation in the threshold beyond which fibers are considered to be at risk of failure.

Carbon fibers, known for their lightweight and high-strength properties, are used in high-performance applications. However, they can fail when subjected to extreme stress beyond their breaking point. PORT-VaR analysis helps:

I. Identify the random threshold stress point where carbon fibers begin to fail,
II. Quantify the risk of extreme stress that could cause a significant portion of fibers to break,
III. Estimate the expected breaking stress beyond the threshold, taking into account variability in material properties or environmental factors.

For instance, engineers might use PORT-VaR to ensure that at a 99% confidence level, no more than 1% of carbon fibers will break under extreme load conditions, thereby optimizing design safety.

On the other hand, glass fibers are used in composites for various industrial applications due to their strength and flexibility. In extreme conditions, the strength of these fibers can vary, and understanding their reliability is crucial. In practical terms, PORT-VaR could help predict that under a certain stress level, only a small percentage of glass fibers will fail, allowing manufacturers to design products with better durability and reliability.

5.5 Reliability and risk analysis

Starting with MO-P analysis, Table 5 offers insights into the analysis of the breaking stress of carbon fibers using the MO-P analysis, an important tool in reliability analysis. The MO-P values increase with increasing order P, which indicates the behavior of the fiber breaking stress data as the order of the analysis shifts. In reliability terms, this could represent how different thresholds or tolerance levels (related to the breaking stress) influence the estimated performance or failure behavior. As P increases, the MO-P values get closer to 1, which implies a more robust and

reliable estimation of breaking stress in industrial applications. It suggests that the breaking stress performance improves or stabilizes under higher thresholds.

The TRM value of 1.657838 serves as a baseline reference point for the average breaking stress across all fibers under study. In a reliability context, this can be used as an overall reliability measure for the batch of carbon fibers.
In industry, the TRM value might be useful for quality control and production benchmarks, helping manufacturers ensure that the fiber meets or exceeds certain strength expectations.

The MSE values decrease with increasing P, showing that the estimates of breaking stress become more accurate as the order P increases. Lower MSE implies that the predicted values are closer to the actual observed values, improving the reliability of the analysis.
For industrial applications, reducing error is critical in precision manufacturing. This information could be used to optimize the production process, where a lower MSE reflects better predictability and control over material performance, particularly in applications where carbon fiber strength is critical (e.g., aerospace, automotive).

The bias values also decrease as P increases, meaning that the estimates become less biased and more reflective of the true breaking stress behavior of the carbon fibers.
In a reliability setting, lower bias improves the trustworthiness of predictions, ensuring that performance metrics like breaking stress are more reliable. In industries relying on carbon fibers for structural integrity, minimizing bias in reliability models can ensure better product consistency and safety.

Thes results of Table 5 represents a statistical evaluation of the breaking stress, which is a crucial metric in determining the reliability of carbon fibers used in high-stress environments. MO-P analysis helps identify the distribution and variability in breaking stress, allowing industries to gauge the longevity and safety of materials under different conditions. In an industrial context, the insights gained from MO-P analysis, MSE, and bias are crucial for setting up quality control standards. By understanding how breaking stress behaves across different orders P, manufacturers can refine their processes to minimize errors and bias, ensuring the production of more reliable and robust carbon fibers. The decreasing trend of bias and MSE in the analysis indicates that higher-order assessments provide better reliability estimates. In industries that require risk assessment for material failure (e.g., construction, aerospace), these insights are valuable for anticipating potential issues and designing better safety protocols.

Figure 7 gives the MO-P analysis for breaking stress of carbon fibers data. Figure 8presents the MO-P analysis for strength of glass fibers data.

Table 5: MO-P analysis under the breaking stress of carbon fibers data.

P	1	2	3	4	5
TRM			1.657838		
MO-P	0.92	0.924	0.9483333	0.960525	0.98062
MSE	0.5444049	0.5385182	0.5033969	0.4862454	0.4586242
Bias	0.737838	0.733838	0.7095047	0.697313	0.677218

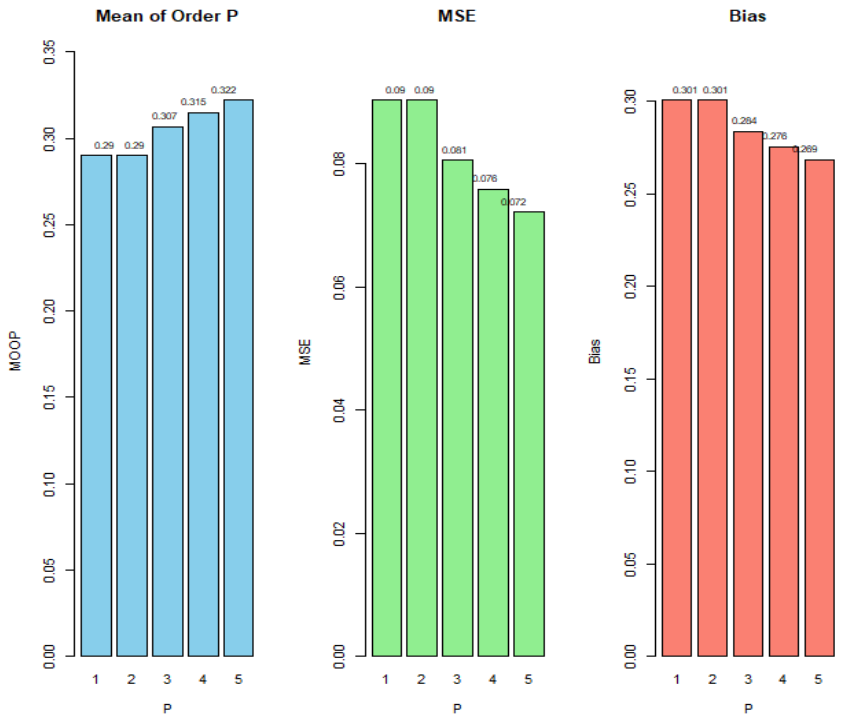

Figure 7: MO-P analysis for breaking stress of carbon fibers data.

Table 6 presents the MO-P analysis under the strength of glass fibers data. Due to Table 6, the MO-P values increase as the order P increases, similar to the breaking stress of carbon fibers, but with slightly higher initial values for glass fibers. This suggests that the performance of glass fibers in terms of strength may show a different reliability trend compared to carbon fibers. For P=1, the MO-P value is 1.014, showing that glass fibers have a baseline higher than 1. The increase in MO-P values as P rises indicates improved reliability as the threshold or tolerance for strength increases. These results help determine how glass fibers perform under varying strength thresholds, which is critical for industries relying on glass fibers for high-performance applications (e.g., construction, telecommunications, aerospace). The MSE values decrease consistently as the order P increases, from 0.3619646 at P=1 to 0.2486368 at P=5. This decline in MSE suggests that higher-order reliability estimates provide better accuracy and predictability for the strength of glass fibers. The bias values decrease from 0.6016349 at P=1 to 0.4986349 at P=5, meaning the estimates become less biased as the order increases. Lower bias indicates that the predicted strength of glass fibers aligns more closely with the actual strength as the order P increases.

The MO-P analysis provides insights into the variability and reliability of glass fibers in terms of strength. The increasing MO-P values indicate that glass fibers become more reliable at higher strength thresholds, which is critical for ensuring the fibers' performance in high-stress applications (e.g., construction materials, fiber optics, aerospace components). In industries that rely on the consistent strength of glass fibers, understanding the MSE and bias metrics is crucial for improving quality control processes. Lower MSE and bias values demonstrate that higher-order models provide more accurate estimates, helping manufacturers produce fibers that meet stringent reliability and safety standards. In applications where glass fibers are used in critical components, such as in architecture or aerospace, the accuracy of strength predictions is vital for assessing risks related to material failure. The reduced bias and MSE with higher P values suggest that higher-order reliability models can provide more precise risk assessments, helping engineers and manufacturers mitigate potential failures and improve material performance.

Table 6: MO-P analysis under the strength of glass fibers data.

P	1	2	3	4	5
TRM			1.615635		
MO-P	1.014	1.0475	1.059	1.0905	1.117
MSE	0.3619646	0.3227773	0.3098424	0.2757667	0.2486368
Bias	0.6016349	0.5681349	0.5566349	0.5251349	0.4986349

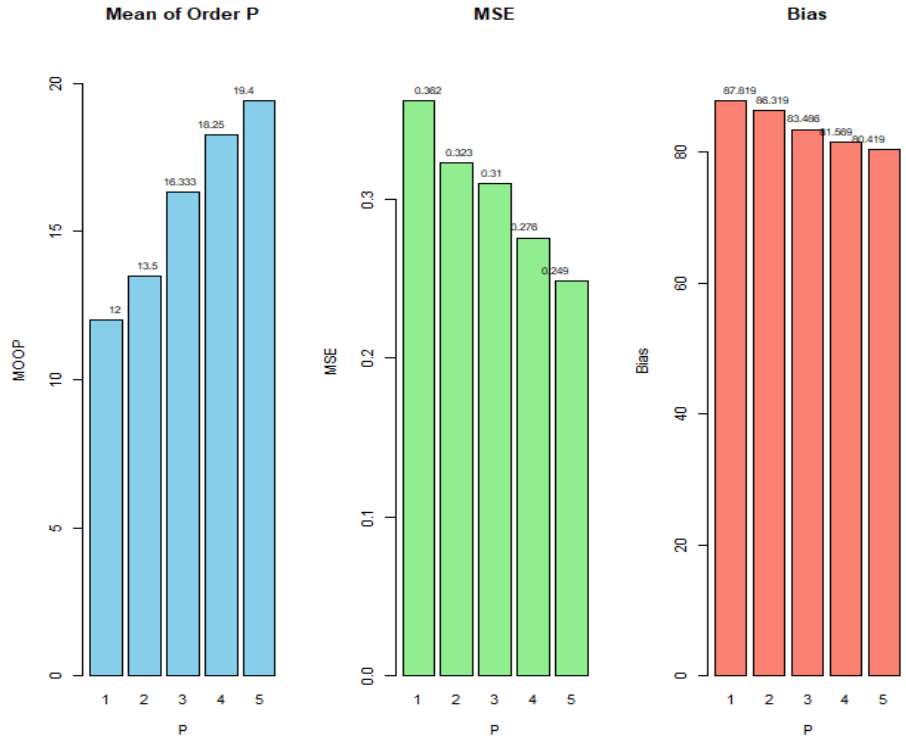

Figure 8: MO-P analysis for strength of glass fibers data.

Table 7 provides the PORT VaR analysis under the medical breaking stress of carbon fibers data. Based on Table 6 we see that:

I. VaR and TVaR increase progressively as the confidence level (CL) rises. The VaR at 95% is 2.69060, while the corresponding TVaR is 3.643458. These increasing values highlight the greater risk associated with extreme stress levels for carbon fibers as we look at higher percentiles of confidence.

II. The number of peaks over VaR also rises with the confidence level. At 55%, we observe 55 peaks, and by 95%, this number rises to 95. This shows a clear correlation between increasing confidence levels and the frequency of extreme stress events exceeding the VaR threshold.

III. For industries using carbon fibers in medical applications (e.g., prosthetics, medical devices), the increasing VaR and TVaR values reflect a critical need to ensure that carbon fiber materials can withstand high-stress conditions reliably. The presence of a significant number of peaks over the VaR threshold at higher confidence levels suggests that the material may be subjected to more frequent stress points in extreme use cases. In high-reliability sectors such as aerospace or healthcare, where failure is not an option, both VaR and TVaR metrics are essential for assessing the risk of material failure under stress. The data from this table can inform engineers about the necessity of building materials that are not only resilient under average conditions but also capable of withstanding extreme, less frequent

stress events. The analysis of these statistical properties can be used to improve quality control in manufacturing, ensuring that carbon fibers are tested rigorously across multiple percentiles of stress and not just average conditions. The analysis could guide testing procedures to focus more on the tail risks (beyond VaR), ensuring that rare but extreme failure points are accounted for in product design.

On the other hand, Figure 9 presents the histograms with VaR and peaks under the breaking stress of carbon. However, Figure 10 (left) shows the density plots of peaks under the breaking stress of carbon and Figure 10 (right)) shows the VaR and TVaR plots of peaks under the breaking stress of carbon.

Table 7: PORT VaR analysis under the medical breaking stress of carbon fibers data.

CL	VaR	TVaR	N. peaks over VaR	Min.	1st Qul.	Median	Mean	3rd Qul.	Max.
55%	1.57455	1.617353	55	1.515	1.608	1.799	1.967	2.030	5.306
60%	1.61480	1.709158	60	1.477	1.580	1.768	1.927	2.022	5.306
65%	1.71345	1.811747	65	1.450	1.552	1.738	1.891	1.987	5.306
70%	1.76440	1.919980	70	1.351	1.531	1.714	1.856	1.981	5.306
75%	1.81450	2.048805	75	1.310	1.504	1.628	1.820	1.958	5.306
80%	1.90240	2.218237	80	1.244	1.476	1.615	1.785	1.905	5.306
85%	2.02140	2.424330	85	1.224	1.450	1.599	1.753	1.884	5.306
90%	2.04330	2.792476	90	1.196	1.393	1.575	1.723	1.829	5.306
95%	2.69060	3.643458	95	1.117	1.334	1.556	1.693	1.822	5.306

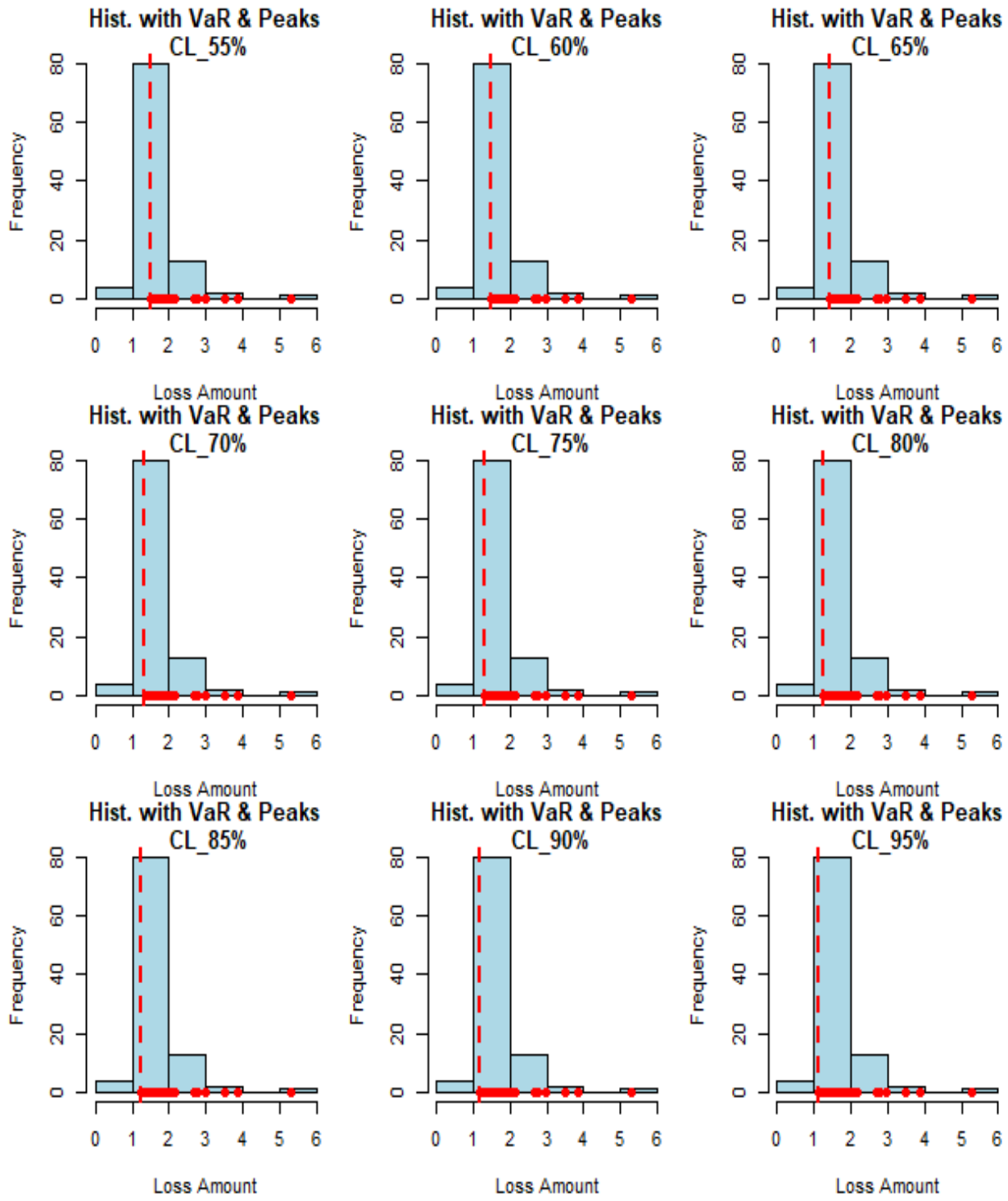

Figure 9: Histograms with VaR and peaks under the breaking stress of carbon.

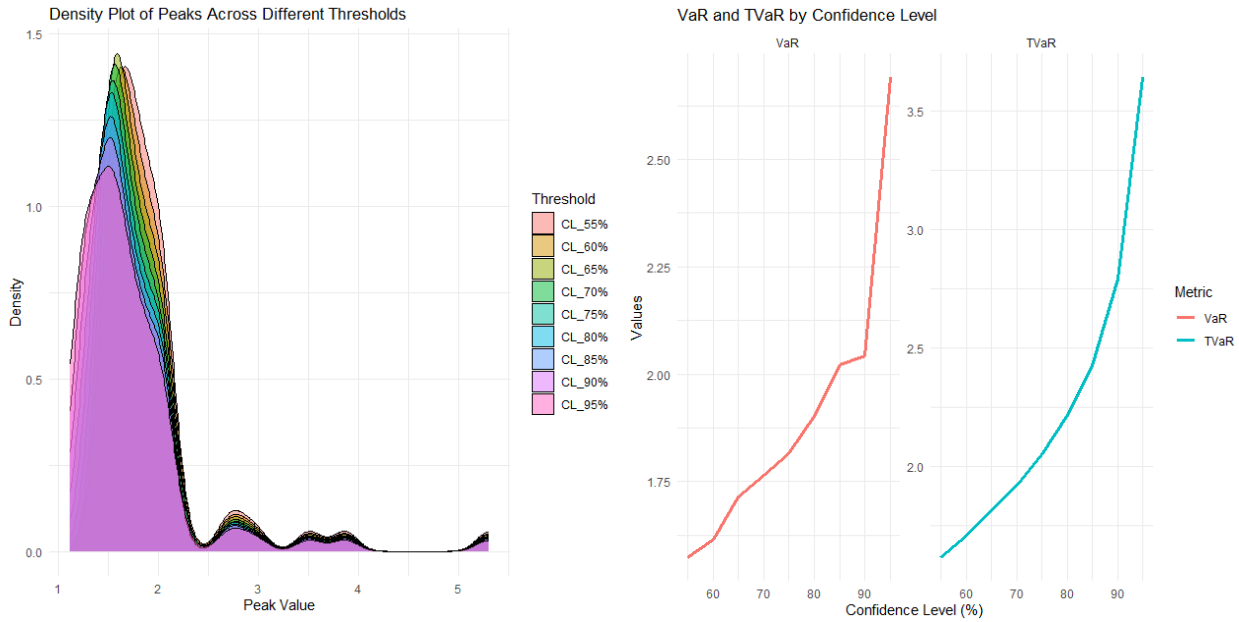

Figure 10: Density plots of peaks under the breaking stress of carbon (left) and VaR and TVaR plots of peaks under the breaking stress of carbon (right).

Table 8 presents the PORT analysis under the medical strength of glass fibers data. Based on the results of Table 8, we note that:

I. The VaR and TVaR values show an upward trend as the confidence level (CL) increases. At 55%, the VaR is 1.5691, while at 95%, it rises to 2.4116. Similarly, the TVaR increases from 1.522143 at 55% to 3.051929 at 95%. These rising values suggest that for glass fibers under medical-strength tests, the risk of failure becomes more prominent at higher stress percentiles. TVaR captures the extreme tail events and indicates that glass fibers could fail more severely in extreme conditions, making it crucial to account for high-stress scenarios in reliability studies.

II. The number of peaks over VaR increases with the confidence level, indicating more frequent extreme stress events as we examine higher percentiles of the data. For example, at 55%, there are 35 peaks over VaR, which rises to 59 peaks at 95%. This pattern highlights that while failures may not be common at lower confidence levels, there is a clear increase in the frequency of extreme failure events as the stress level increases. This information is critical for industries using glass fibers in medical devices, where even occasional failures under stress can have severe consequences.

For supporting our financings, we presented Figure 12 with displays the density plots of peaks under the strength of glass fibers (left) and VaR and TVaR plots of peaks under the strength of glass fibers (right).

Table 8: PORT analysis under the medical strength of glass fibers data.

CL	VaR	TVaR	N. peaks over VaR	Min.	1st Qul.	Median	Mean	3rd Qul.	Max.
55%	1.5691	1.522143	35	1.501	1.586	1.731	1.862	1.877	4.121
60%	1.5914	1.597008	38	1.476	1.571	1.698	1.832	1.874	4.121
65%	1.6672	1.680690	42	1.426	1.535	1.684	1.804	1.867	4.121
70%	1.6962	1.768680	44	1.364	1.520	1.668	1.775	1.821	4.121
75%	1.7410	1.872592	47	1.306	1.492	1.602	1.748	1.803	4.121
80%	1.7828	2.011023	50	1.288	1.477	1.592	1.721	1.789	4.121
85%	1.8733	2.187934	53	1.276	1.459	1.581	1.696	1.757	4.121
90%	1.9148	2.464412	56	1.271	1.401	1.573	1.673	1.750	4.121
95%	2.4116	3.051929	59	1.223	1.363	1.541	1.651	1.748	4.121

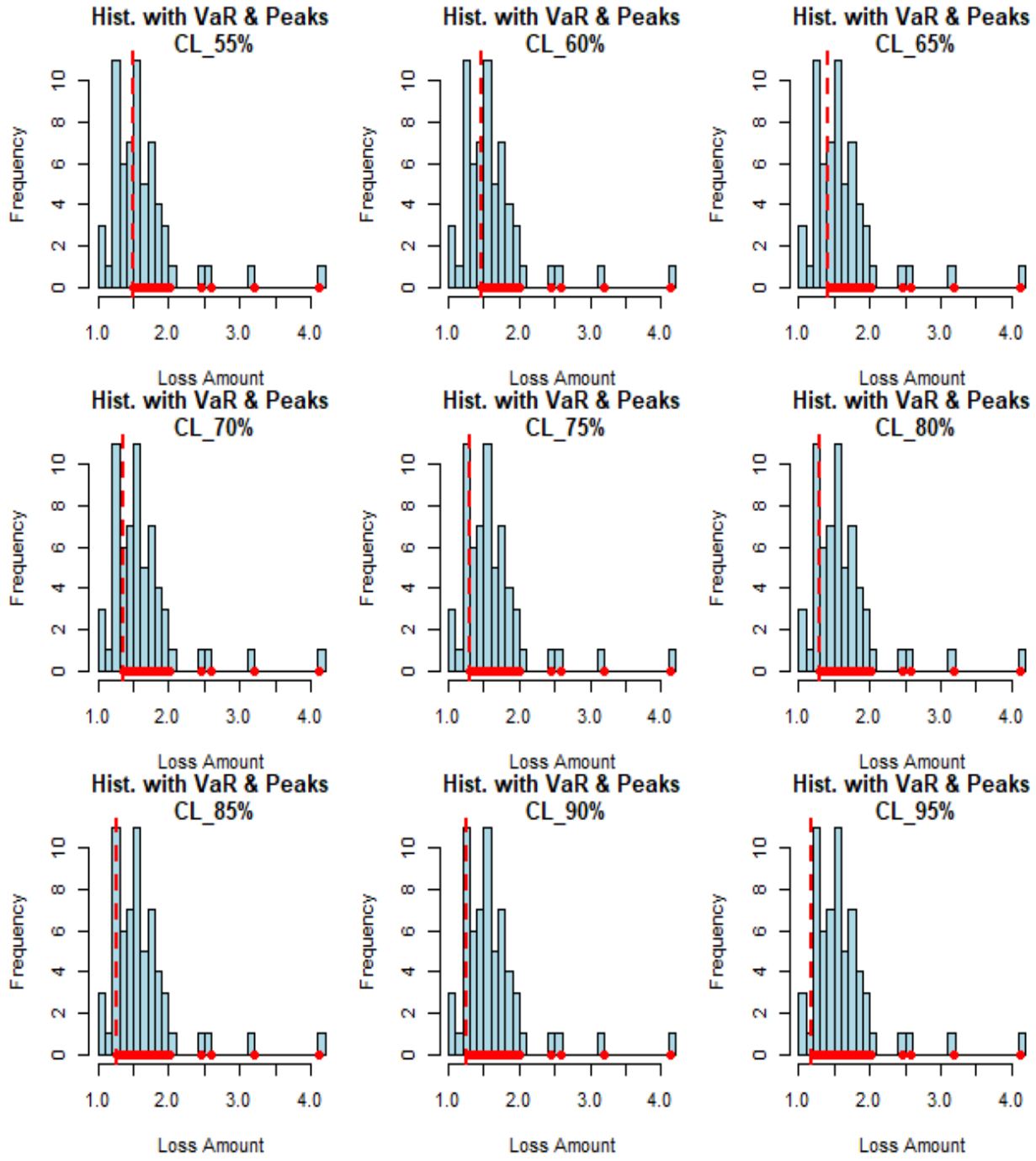

Figure 11: Histograms with VaR and peaks under the strength of glass fibers.

For industries relying on glass fibers for medical applications (e.g., sutures, implants, prosthetics), the increasing VaR and TVaR values reflect the growing risk of material failure under high stress. This is particularly important when designing components that need to withstand sustained loads or sudden impacts in medical environments. The TVaR metric provides a more comprehensive picture of extreme stress events than VaR alone. By understanding the expected losses beyond the VaR, engineers and designers can develop better mitigation strategies, ensuring that glass fibers perform reliably even under the most extreme use cases. The consistent maximum value of 4.121 across all confidence levels suggests that while average and median values decline at higher confidence levels, extreme failure events do not become less severe. This emphasizes the importance of accounting for tail behavior in quality control, ensuring that the rare but extreme breaking points are considered in the production and testing of glass fibers. The findings from this PORT analysis provide critical insights into the failure behavior of glass fibers used in medical devices. Given that such devices often operate in high-stress environments where failure is not an option, understanding the statistical behavior of materials at higher confidence levels is crucial for improving product design, safety, and reliability.

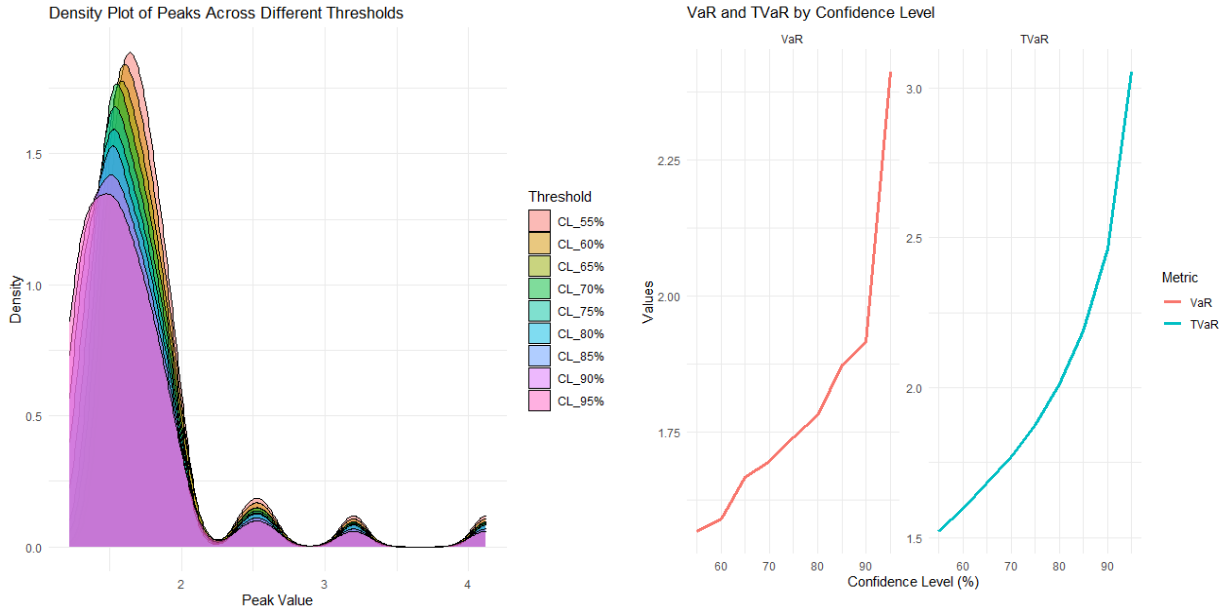

Figure 12: Density plots of peaks under the strength of glass fibers (left) and VaR and TVaR plots of peaks under the strength of glass fibers (right).

6. Conclusions

Peaks over a random threshold value-at-risk (PORT-VaR) analysis serves as a robust methodology for assessing extreme value reliability data, particularly pertinent to materials such as carbon and glass fibers. This analytical approach enhances the traditional frameworks of value at risk (VaR) and tail value at risk (TVaR) by integrating random thresholds, thereby allowing for a more refined understanding of material behavior under extreme conditions. Such insights are crucial in fields where material failure can result in significant financial losses or pose safety risks, including aerospace, automotive, and civil engineering sectors. The utility of PORT-VaR extends beyond just material science; it intersects meaningfully with medical applications as well. By integrating Mean of Order P (MO-P) analyses with VaR and PORT-VaR, healthcare professionals can gain significant insights into risk evaluation and patient management strategies. For instance, examining both the average and extreme strength characteristics of glass fibers enables medical professionals to develop more effective treatment plans tailored to individual patient needs. This focus on extreme values not only enhances patient outcomes but also improves the overall quality of care provided.

Furthermore, the proposed reliability analysis highlights how the PORT-VaR methodology can be applied to medical breaking stress data, underscoring the value of this approach in evaluating the performance and reliability of medical

materials. By thoroughly analyzing these extreme value data, practitioners can make informed decisions about material selection, ultimately leading to innovations in medical device design and patient safety.

To illustrate our primary objective and facilitate a deeper medical analysis, we introduced a novel extreme value model named the generalized Rayleigh reciprocal-Weibull (GR-RW), accompanied by its key mathematical results. The introduction of this model allows for a better fitting of the data and a more comprehensive understanding of the underlying phenomena associated with material reliability and performance. Additionally, we conducted a simulation study and analyzed two real datasets to compare competing models, providing empirical evidence for the effectiveness of our proposed approach.

In conclusion, the integration of PORT-VaR, VaR, and MO-P analyses offers a multifaceted perspective on both material reliability and patient care. The insights gleaned not only highlight the advantages of using advanced statistical models in evaluating extreme values but also underscore the potential for improved decision-making in critical applications. As industries continue to advance, particularly in the fields of aerospace, automotive, and healthcare, the implementation of such comprehensive analytical frameworks will be vital for driving innovations and enhancing safety and reliability standards.

References

1. Acerbi, C., & Tasche, D. (2002). On the coherence of expected shortfall. Journal of banking & finance, 26(7), 1487-1503.
2. Afify, A. Z., Yousof, H. M., Cordeiro, G. M., Ortega, E. M., & Nofal, Z. M. (2016). The Weibull Fréchet distribution and its applications. Journal of Applied Statistics, 43(14), 2608-2626.
3. Ahmed, B., & Yousof, H. (2023). A new group acceptance sampling plans based on percentiles for the Weibull Fréchet model. Statistics, Optimization & Information Computing, 11(2), 409-421.
4. Al-babtain, A. A., Elbatal, I., & Yousof, H. M. (2020a). A New Flexible Three-Parameter Model: Properties, Clayton Copula, and Modeling Real Data. Symmetry, 12(3), 440.
5. Smith, R. L., & Naylor, J. (1987). A comparison of maximum likelihood and Bayesian estimators for the three-parameter Weibull distribution. Journal of the Royal Statistical Society Series C: Applied Statistics, 36(3), 358-369.
6. Al-Babtain, A. A., Elbatal, I., & Yousof, H. M. (2020b). A new three parameter Fréchet model with mathematical properties and applications. Journal of Taibah University for Science, 14(1), 265-278.
7. Alizadeh, M., Afshari, M., Contreras-Reyes, J. E., Mazarei, D., & Yousof, H. M. (2024). The Extended Gompertz Model: Applications, Mean of Order P Assessment and Statistical Threshold Risk Analysis Based on Extreme Stresses Data. IEEE Transactions on Reliability, doi: 10.1109/TR.2024.3425278.
8. Almazah, M.M.A., Almuqrin, M.A., Eliwa, M.S., El-Morshedy, M., Yousof, H.M. (2023). Modeling Extreme Values Utilizing an Asymmetric Probability Function. *Symmetry* 2021, *13*, 1730. https://doi.org/10.3390/sym13091730
9. Bjerkedal, T. (1960). Acquisition of Resistance in Guinea Pies infected with Different Doses of Virulent Tubercle Bacilli.
10. Chakraborty, S., Handique, L., Altun, E., & Yousof, H. M. (2019). A New Statistical Model for Extreme Values: Properties and Applications. Int. J. Open Problems Compt. Math, 12(1).
11. Elbatal, I., Diab, L. S., Ghorbal, A. B., Yousof, H. M., Elgarhy, M., & Ali, E. I. (2024). A new losses (revenues) probability model with entropy analysis, applications and case studies for value-at-risk modeling and mean of order-P analysis. AIMS Mathematics, 9(3), 7169-7211.
12. Elgohari, H. and Yousof, H. M. (2021). A New Extreme Value Model with Different Copula, Statistical Properties and Applications. Pakistan Journal of Statistics and Operation Research, 17(4), 1015-1035. https://doi.org/10.18187/pjsor.v17i4.3471
13. Elsayed, H. A. H., & Yousof, H. M. (2020). The generalized odd generalized exponential Fréchet model: univariate, bivariate and multivariate extensions with properties and applications to the univariate version. Pakistan Journal of Statistics and Operation Research, 529-544.
14. Hamedani, G. G. and Maadooliat, M. (2021). Extreme Value Theory Applications in Medical and

Healthcare Studies: A Review. Journal of Statistical Theory and Applications, 20(3), pp. 91–115.
15. Haq, M. A. ul, Yousof, H. M., & Hashmi, S. (2017). A New Five-Parameter Fréchet Model for Extreme Values. Pakistan Journal of Statistics and Operation Research, 13(3), 617-632.
16. Harrison, R. L. and Marden, J. I. (2020). The Role of Extreme Value Theory in Modeling Disease Outbreaks: Applications to COVID-19. Journal of Biostatistics, 18(4), pp. 425–440.
17. Ibrahim. M., Handique, L., Chakraborty, S., Butt, N. S. and M. Yousof, H. (2021). A new three-parameter xgamma Fréchet distribution with different methods of estimation and applications. Pakistan Journal of Statistics and Operation Research, 17(1), 291-308. https://doi.org/10.18187/pjsor.v17i1.2887
18. Jahanshahi, S.M.A., Yousof, H. M. and Sharma, V.K. (2019). The Burr X Fréchet Model for Extreme Values: Mathematical Properties, Classical Inference and Bayesian Analysis. Pak. J. Stat. Oper. Res., 15(3), 797-818.
19. Korkmaz, M. Ç., Yousof, H. M., & Ali, M. M. (2017). Some theoretical and computational aspects of the odd Lindley Fréchet distribution. İstatistikçiler Dergisi: İstatistik ve Aktüerya, 10(2), 129-140.
20. Kotz, S., & Nadarajah, S. (2000). Extreme value distributions: theory and applications. world scientific.
21. Minkah, R., de Wet, T., Ghosh, A., & Yousof, H. M. (2023). Robust extreme quantile estimation for Pareto-type tails through an exponential regression model. Communications for Statistical Applications and Methods, 30(6), 531-550.
22. Salah, M. M., El-Morshedy, M., Eliwa, M. S. and Yousof, H. M. (2020). Expanded Fréchet Model: Mathematical Properties, Copula, Different Estimation Methods, Applications and Validation Testing. Mathematics, 8(11), 1949.
23. Shrahili, M.; Elbatal, I. and Yousof, H. M. (2021). Asymmetric Density for Risk Claim-Size Data: Prediction and Bimodal Data Applications. Symmetry 2021, 13, 2357. https://doi.org/10.3390/sym13122357
24. Tasche, D. (2002). Expected shortfall and beyond. Journal of Banking & Finance, 26(7), 1519-1533.
25. Wang, S. Y. and Hu, W. L. (2019). Applications of Fréchet Distribution in Medical Device Reliability Analysis. Reliability Engineering & System Safety, 187, pp. 12–23.
26. Wingo, D. R. (1983). Maximum likelihood methods for fitting the Burr type XII distribution to life test data. Biometrical journal, 25(1), 77-84.
27. Wirch, J. L. (1999). Raising value at risk. North American Actuarial Journal, 3(2), 106-115.
28. Yousof, H. M., Afify, A. Z., Abd El Hadi, N. E., Hamedani, G. G., & Butt, N. S. (2016). On six-parameter Fréchet distribution: properties and applications. Pakistan Journal of Statistics and Operation Research, 281-299.
29. Nichols, M. D., & Padgett, W. J. (2006). A bootstrap control chart for Weibull percentiles. Quality and reliability engineering international, 22(2), 141-151.
30. Yousof, H. M., Altun, E., & Hamedani, G. G. (2018a). A new extension of Fréchet distribution with regression models, residual analysis and characterizations. Journal of Data Science, 16(4), 743-770.
31. Yousof, H. M., Butt, N. S., Alotaibi, R. M., Rezk, H., Alomani, G. A., & Ibrahim, M. (2019). A new compound Fréchet distribution for modeling breaking stress and strengths data. Pakistan Journal of Statistics and Operation Research, 15(4), 1017-1035.
32. Yousof, H. M., Hamedani, G. G., & Ibrahim, M. (2020). The Two-parameter Xgamma Fréchet Distribution: Characterizations, Copulas, Mathematical Properties and Different Classical Estimation Methods. Contributions to Mathematics, 2 (2020), 32-41.
33. Yousof, H. M., Jahanshahi, S. M. A., Ramires, T. G., Aryal, G. R., & Hamedani, G. G. (2018b). A new distribution for extreme values: regression model, characterizations and applications. Journal of Data Science, 16(4), 677 -706.
34. Yousof, H. M., Rasekhi, M., Altun, E., & Alizadeh, M. (2018c). The extended odd Fréchet family of distributions: properties, applications and regression modeling. International Journal of Applied Mathematics and Statistics, 30(1), 1-30.
35. Yousof, H.M.; Tashkandy, Y.; Emam, W.; Ali, M.M.; Ibrahim, M. (2023). A New Reciprocal Weibull Extension for Modeling Extreme Values with Risk Analysis under Insurance Data. Mathematics 2023, 11, 966. https://doi.org/10.3390/ math11040966